Photochromism in inorganic crystallised compounds

Yazan Badour, Veronique Jubera, Inès Andron, Christine Frayret, Manuel Gaudon

Optical Materials: X 12 (2021) 100110

Contents lists available at ScienceDirect

Optical Materials: X

journal homepage: www.journals.elsevier.com/optical-materials-x

Photochromism in inorganic crystallised compounds

Y. Badour [a], V. Jubera [a,*], I. Andron [a], C. Frayret [b,c], M. Gaudon [a]

[a] Univ. Bordeaux, CNRS, Bordeaux INP, ICMCB, UMR5026, F-33600, Pessac, France
[b] Laboratoire de Réactivité et Chimie des Solides (LRCS), UMR CNRS 7314, Université de Picardie Jules Verne, Hub de l'Energie, 15 Rue Baudelocque, 80000, Amiens Cedex, France
[c] Réseau sur le Stockage Electrochimique de l'Energie (RS2E), France

ARTICLE INFO

Keywords:
Photochromism
Transition metal oxide
Rare earth element
Colour switch

ABSTRACT

Photochromism is a phenomenon describing the irradiation-induced reversible transformation of a chemical compound's colour between two states (dubbed as colour switch). This review makes an up-to-date account of inorganic photochromic compounds. In the first part, we summarise the photochromic mechanisms involving transition metal oxides, with an emphasis on the canonical WO_3 large-bandgap semiconductor. In the second part, we discuss the potential contribution of rare earth elements to the widening of the colourimetric contrasts in absorption, as well as the method of modulation in emission.

1. Introduction

1.1. Materials of interest

Colour is the visual perception of the appearance of a material's surface based on, without being strictly linked to, the spectral distribution of light stimulating specific nerve cells, called cones, located on the retina. The colour phenomena occurring in materials (here regarded in the sense of solid matter) can be classified according to two fundamental aspects of nature (Fig. 1): (1) physical phenomena, such as diffusion, refraction, interference, *etc.*, which are more related with the architectural scale of matter rather than its chemical composition, and (2) chemical phenomena, which are primarily determined by electronic transfer, and by extension related to the chemical composition and elemental organisation at the atomic (crystallographic) scale, the colour being the trace left by the travel of the electrons. Furthermore, it is essential to make a distinction between (i) the process of emission, where the object acts as the primary source of light, actively generating its colour *via* "physical" incandescence and "chemical" luminescence, producing a white colour through the accumulated irradiance of all visible colours, and (ii) the mechanisms of absorption/reflection/diffusion, where the "subtraction" of visible colours emitted from a standard illuminant on a material object's surface produces black colouration. In this review, we approach the mechanisms of photochromism and photochromo-luminescence in material objects from the respective aspects of light absorption/reflection and emission, while restricting our assessment to phenomena of chemical origin only. Another fundamental aspect of nature affecting such phenomena, are the inherent disparities between organic and inorganic matter. In this regard, apart from a few words in the introductory chapter, this review is primarily intended to discuss the phenomenon of photo-colouration in mineral matter.

In the first part, the photochromic mechanisms involving transition metal elements, with a focus on the WO_3 compound, are reported. In the second part, the potential contribution of rare earth elements to the widening of the colourimetric contrast properties in absorption, as well as the method of modulation in emission, will be elaborated on.

1.1.1. Colour as a result of chemical absorption

When electron excitation is caused by incident photons, whose energy corresponds to light in the visible range between the grounded and excited states, the material partially absorbs these photons and displays a colour that is specific to its nature. In this case, the de-excitation generally manifests in a non-radiative manner *via* phonon vibrations (unlike luminescence, which corresponds to radiative de-excitation with emission of photons). There are two classes of compounds that meet these characteristics (Fig. 2): the first class concerns dyes, such as anthocyanin or malachite green, which are soluble in a dispersive medium and are almost exclusively of organic origin; the second class relates to pigments (such as smalt, cinnabar, vermilion, or ochre), which are insoluble in dispersive media and are typically of inorganic nature (even if several organic compounds can, however be used as pigments). Notably, both organic dyes and inorganic pigments are capable of

* Corresponding author.
E-mail address: veronique.jubera@u-bordeaux.fr (V. Jubera).

https://doi.org/10.1016/j.omx.2021.100110
Received 19 July 2021; Received in revised form 21 October 2021; Accepted 1 November 2021
Available online 15 November 2021

exhibiting photochromic phenomena.

1.1.2. Chemical luminescence

Unlike incandescence ("warm" light emission), the luminescence ("cold" light emission) of a compound depends directly on the chemical composition of the emissive material. The illuminant medium absorbs energy (supplied by an external source) and then transitions into an excited state, before returning to its initial state by emitting electromagnetic radiation in the form of photon emission. In most cases, these are electronic transitions that occur either within single atoms (or cations, in ionic crystals), which are referred to as intra-atomic transitions, or between the valence band (VB) and the conduction band (CB) in semiconductors, which are then referenced as inert-atomic electronic transitions. Depending on the source (Y) causing the excitation, several types of luminescence can be identified. The materials of the source are called Y-luminescent materials. The main sources of excitation are temperature (thermo-luminescence), electric field (electroluminescence), chemical reactions (chemo-luminescence), pressure (piezo-luminescence), and photons (photo-luminescence). Photo-chromo-luminescence, which will be further developed in this review, relates only to the last case.

1.2. Photochromism: historic overview

The phenomenon of photochromism was first discovered in the late 1870s. The capacity to change colouration under UV light excitation, known as "phototropy", was studied for the first time in 1899 by the Dr. Willy Marckwald, when he published his work concerning the reversible colour change of a ketone of the naphthalene family [1]. This term has been used by the scientific community for over 50 years. In 1950, the Israeli physical chemist Yehudah Hirshberg introduced the word "photochromy", originating from the Greek routes *phos* (light) and *chroma* (colour), which he used to describe the reversible colouration of colourless bianthrone ($C_{28}H_{16}O_2$)-derived compounds under ultraviolet irradiation [2,3]. Thus, for twenty years, these two terms coexisted in the literature, while designating the same phenomenon. In 1970, after a symposium between more than 250 photochemists, the use of only one of these two terms was decided, and "phototropism" was abandoned [4]. A third term emerged around 1920: "tenebrescence", derived from the Latin *tenebrae* (darkness, obscurity), which is exclusively used to describe photochromism in mineralogy.

The opto-electronic mechanisms underlying photochromism have been continuously inciting significant scientific interest ever since, as evidenced by the increasing number of publications since the 1970s (Fig. 3).

1.3. Different classes of photochromic compounds

Photochromism generally designates any reversible change in the colouration of a material from a thermodynamically stable state A to a metastable state B, that is induced by electromagnetic radiation (Fig. 4). The typical metastability of the B state is associated with a longer return to the stable state A, whether this return occurs naturally, or *via* an activation process (*e.g.*, thermally, by immersion in a particular atmosphere, by irradiation at a new wavelength, *etc.*). In most photochromic materials, ultraviolet (UV) radiation is absorbed by state A (at hc/l_A) in the absorbing wavelength range (ideally, at the maximal molar extinction coefficient e_A), thereby causing a change to state B. The return from state B to state A can be realised *via* irradiation-induced excitation at a new wavelength (l_B). The A and B states are energetically separated by a potential energy barrier (ΔE).

The classification of photochromes is generally based on the type of stimulus that enables the reversion reaction (B → A) to manifest. Knowing that the A → B transformation is always photoactivated, there are several ways to revert to the initial state. Under a low potential energy barrier (ΔE), the return reaction can be thermally activated and

Fig. 1. Classification of diverse materials depending on the aspects of physical/chemical colours, primary/secondary light sources, and inorganic/organic compounds: cigarette, tungsten filament bulb, labradorite opal, morpho wings, hackmanite, protoplasts with fluorescein, coloured stones and vegetable basket. (For interpretation of the references to colour in this figure legend, the reader is referred to the Web version of this article.)

Fig. 2. Organic dyes and inorganic pigments demonstrating a large colour spectrum. (For interpretation of the references to colour in this figure legend, the reader is referred to the Web version of this article.)

the photochrome is classified as type T [6]. The return to state A is spontaneous, owing to the metastability of state B, but often sluggish (between a few hours and a few days); however, it can be accelerated by temperature. On the contrary, under higher potential energy barriers, this reaction can only be photoactivated by a second specific irradiation, where the photochrome is classified as type P [5]. Under sufficient irradiation, switching between states A and B is usually very fast (picosecond duration times). A simple way to distinguish between the two photochromic compound types discussed above is that in type T thermal transformations are involved, whereas in type P purely photochemical mechanisms are involved.

In most photochromic compounds, the stable state A is initially colourless or pale, and becomes darkened once it transforms into state B under irradiation; this is positive photochromism. As an illustration, a wide variety of colourations were achieved for compounds derived from the diarylethene family after UV exposure (Fig. 5a). Another illustration of positive photochromism is exhibited by the Hackmanite-type ore ($Na_8[AlSiO_4]_6Cl_{1.8}S_{0.1}$), where the amethyst colouration manifests after UV irradiation ($\lambda = 365$ nm) (Fig. 5b). This material can revert to its initial colouration rapidly, *via* photo- or thermo-activation, or slowly, when left in the dark [7,8].

In the minority of cases, the already coloured compound can sustain photobleaching under visible irradiation, and becomes completely incapable of neither negative, nor reverse photochromism. This phenomenon has been reported to date only for rare organic or hydride compounds. Barachevsky et al. have reported in a review that most studies on negative photochromism focus on spiro bicyclic organic compounds (in which the two cycles, spiropyran and spirooxazine, are connected by a single atom), that were initially coloured owing to the presence of merocyanine [9,10]. For example, Yamaguchi et al. (Fig. 5c) demonstrated that a red-coloured hybrid composed of a merocyanine adsorbed on a mesoporous silica fibre lost its colouration upon exposure to visible radiation [10]. The obtained colourless compound, comprising a spiropyran combined with organophilic clay, exhibited better reversibility of the photochromism process, as evidenced by the compound recovering its red colour after being kept approximately 10 h in the dark. Furthermore, the restoration of the initial colouring could be accelerated by heat treatment. Accordingly, numerous studies on negative photochromism have focused on diarylethene-type compounds or thioindigo-type dyes ($C_{16}H_8O_2S_2$) [9,11,12].

1.4. Applications of inorganic photochromic compounds

Ophthalmic lenses and glass building facades are among the most prominent practical applications of photochromism. Recently, a new cost-effective smart facade glazing has been developed which darkens in a reversible way under intense sunlight, thereby protecting the eyes from UV radiation, while allowing better control of solar illumination in buildings (Fig. 6a and b). Additionally, stemming from their thermal barrier and UV protection layer features, photochromic building panels and car windows present significant potential in reducing the overall energy consumption of modern buildings and cars, while improving safety [14].

The first inorganic photochromic lens model appeared in the 1970s and was marketed by Corning Inc. under the name “PhotoSun®“, and a few years later “PhotoGray®“. This model consisted of borosilicate glass doped with monovalent copper containing silver salts. The dark tint in these mineral glasses is derived from the precipitation of silver halide particles (chloride or bromide, on the order of 100 Å) under UV irradiation, which are dispersed in the glass during its manufacture. Under the effect of UV rays, the following oxidation-reduction reaction takes place: $Ag^+ + Cu^+ \rightarrow Ag^0 + Cu^{2+}$ [15,16]. The metallic silver aggregates (~20 nm) that form on the surface of the silver halide particles absorb light and give a dark colour to the material. In the dark, the material

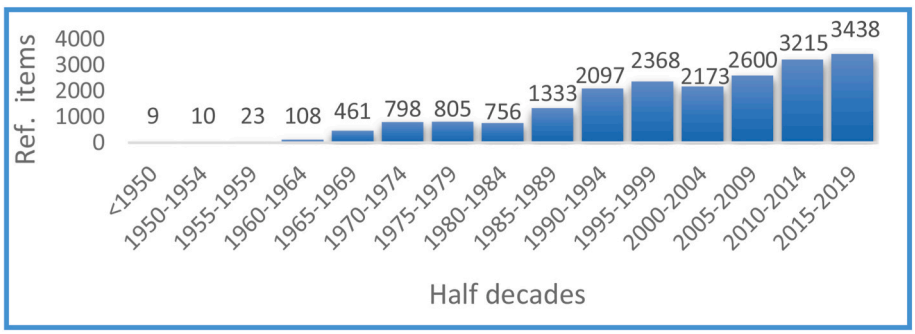

Fig. 3. Historic catalogue of the number of items pertaining to “photochromism” extracted from the sci-Finder database.

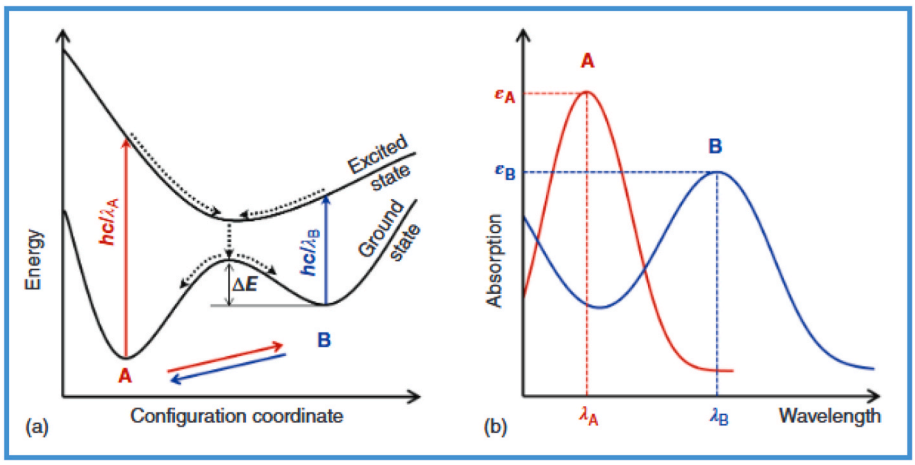

Fig. 4. Bidirectional reaction induced by an electromagnetic excitation between two molecular/crystal states, A and B: (a) Diagram of potential energies and (b) associated absorption spectra [5].

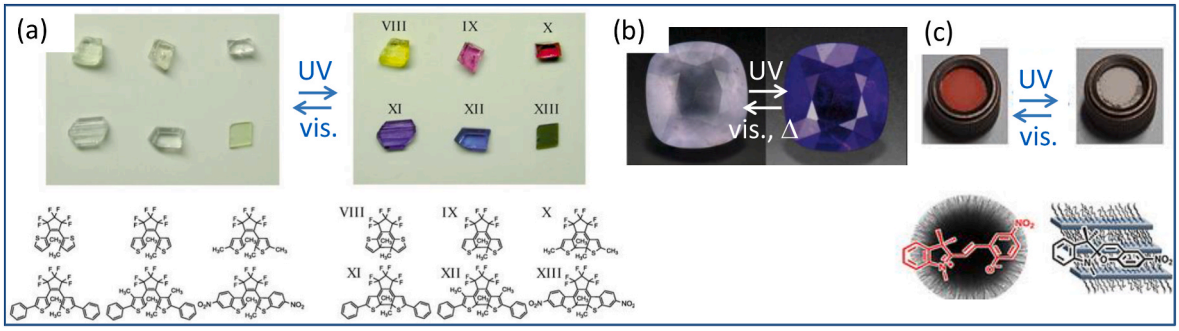

Fig. 5. (*a*) Crystals from a diarylethene derivative before (left) and after (right) UV radiation [13]. (b) Hackmanite stone from Burma before (left) and after exposure (right) to UV radiation (365 nm) [8]. (c) Reversible photochromism of a red merocyanine transforming into a colourless spiropyran upon exposure to visible radiation [10]. (For interpretation of the references to colour in this figure legend, the reader is referred to the Web version of this article.)

returns to its original tint *via* a reverse reaction. Thermal agitation or irradiation in the visible region can accelerate the photobleaching process.

Inorganic transition optical lenses were dethroned in the 1990s by their organic counterparts for various reasons [17]: on one hand, the thicker parts of the mineral glass exhibited deeper darkening than the thinner parts, often resulting in a visually heterogeneous colouration. On the other hand, the more fragile and heavier inorganic glasses used for this technology (borosilicate glasses density = 3.21) could hardly compete with the comfort provided by organic lenses (density ~ 1.2). Organic lenses are made of transparent polymers (*e.g.*, poly di (ethylene glycol) bis (allyl carbonate)) or polycarbonates, where the photochromic molecules are dispersed inside the lens. These molecules, which comprise a carbon ring, are generally derived (according to Winder et al.) from the families of spironaphthoxazines or chromenes (naphthopyran and benzopyran) [18], and they all follow the same photochromism key mechanism, which is dependent on the latitude for opening and closing the carbon cycle.

Other practical applications taking advantage of the electromagnetic irradiation-triggered smart colour change mechanism are aesthetic-related, such as photochromic dyes. For instance, the French company Euracli offers a range of products called EuraChrom®, consisting of three basic photochromic dyes (blue, red, yellow) which can be mixed with other non-photochromic dyes to produce a wide colour palette. Additionally, Vivimed offers a range of organic dyes called Reversacol™, which are supplied in the form of polycrystalline powders. Similarly, photochromic inks and varnishes for application on a variety of substrates are commercially available, such as the photochromic nail polish offered from the Cattie Girl brand (Fig. 6c). Notably, a patent on water-based photochromic varnishes was filed in 2019 [19]. Morel et al. showed that many advances have been made in the design of photochromic materials for hair dyeing [20]. Indeed, photochromic coating dyes, such as Jarocol® and custom SolarActive® brand t-shirts, have recently become commercially available (Fig. 6d).

The unique feature of UV irradiation-induced colour change has also been exploited for more "technological" functional applications. One such instance is security ink, which can realize optically variable patterns on paper that are difficult to forge, for document authentication purposes [21]. In particular, the Semlex company offers passports with patterns drawn using photochromic ink (Fig. 6e). Another example in this category is a smart cheap bracelet that can control the rate of UV irradiation (Fig. 6f).

Other niche applications have accordingly been reported. Akiyama et al. proposed using europium (Eu)-doped $BaMgSiO_4$ photochromic materials with an apatite-like structure as photo-sensors [22]. Other researchers have reported photochromic materials that can be used as reversible holographic systems [23–25]. A noteworthy common target application is the use of photochromic compounds for high-density optical data storage, an idea initially proposed in 1956 by Hirshberg et al. [3]. This application exclusively concerns P-type photochromic compounds, since only a very brief irradiation (microseconds) allows information to be stored, and this information remains stable until a second irradiation. In addition, it is necessary for the initial state to be restored for a very short time duration. Thus, the cycle must be reversible and indefinitely repeatable, and must be completed rapidly. Remarkably, as early as 1967, Smith et al. proposed a technique for

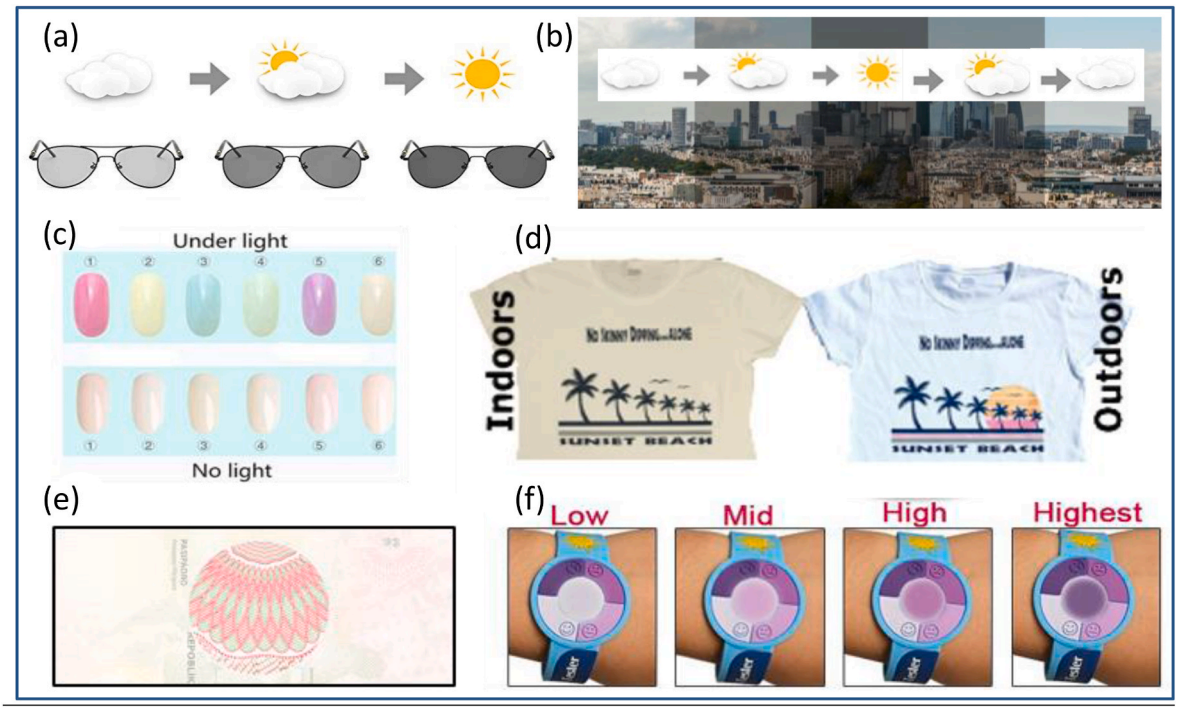

Fig. 6. Diverse applications of photochromic compounds: (a) Photochromic lens (TJUTR Brand); (b) Photochromic smart windows; (c) Cattie Girl brand varnishes; (d) SolarActive® inks printed on a t-shirt; (e) a pattern designed with photochromic ink (Semlex); (f) a bracelet (Xiamen Guzhan Industry & Trade Co.) measuring the rate of UV radiation.

bimodal data storage using silver halide-doped glasses [26]. An improvement of this storage medium has been suggested by Zhang et al., who asserted that three different states can exist if two photochromes are linked, thereby enabling tri-modal storage [27]. This application can be further enriched by synergistically combining photochromism with the inherent properties of the active material, allowing for the realisation of complex devices that are alternately triggered by two different external stimuli, such as light and electric current [28,29].

However, few studies have discussed the influence of photochromism on a material's physical or chemical properties, such as the refractive index, dielectric constant, electrical conductivity, solubility, viscosity, and surface wettability. For example, Agranat and Yacoby demonstrated a correlation between the change in the dielectric constant (responsible for the photorefractive effect) and photochromism in KTa1-xNbxO3 perovskites [30].

Finally, in regard to negative photochromism, where the photobleaching process occurs under UV-light irradiation, whereas the darkening mechanism self-operates without illumination, Barachevsky et al. argued that new materials exploiting this feature could achieve improved performance in applications dedicated to data storage [9]. This advantageous optical property also makes it possible to develop smart camouflage clothing or coatings that lighten up or darken depending on the exterior brightness, for use in the military. These functionalities can also be integrated into consumer applications, such as photo-controlled paints for cars that are capable of reflecting more light under high sun exposure, thereby contributing to temperature regulation within the vehicle.

2. Contribution of transition metal oxides (TMOs) to photochromism

2.1. A case study on WO_x

Over the last several decades, tungsten oxide compounds (WO_x) have been intensively investigated owing to their interesting photochromic properties and structural versatility, which give rise to promising potential applications including optical devices, gas sensors, photocatalysts, flat panel displays, and field emission devices.

In this chapter, the electronic and crystalline structure, viable synthetic methods, technical challenges, and potential applications of WO_x will be discussed over a background of recent literature.

2.1.1. Structure of WO_x

Stoichiometric tungsten trioxide (WO_3) is an n-type indirect bandgap semiconductor with a bandgap ranging between 2.6 and 3.52 eV. Various distorted MO_3-like structures exist [31], in which every off-centre W atom is surrounded by a regular octahedron that is formed by the six nearest O atoms (Fig. 7) [32–34]. The prototype crystal structure of WO_3 is the same as that of cubic ReO_3, where a three-dimensional network is established *via* the corner-sharing of WO_6-octahedra (Fig. 7a). Interestingly, WO_3 can be formed sequentially in six additional phases, which have been identified as follows: monoclinic II (ε-WO3), triclinic (δ-WO_3), monoclinic I (γ-WO_3), orthorhombic (β-WO3), tetragonal (α- WO3), and hexagonal (h-WO3) (Fig. 7b, Table 1).

The seven phases of WO_3 can be differentiated by tilting the angles and distortions of the WO_6 octahedra from the ideal cubic structure, thereby resulting in lower symmetries (Fig. 8). The crystal phase transitions occur in the following sequence, where the stability domains of the various allotropic forms at different temperatures can be determined: monoclinic (ε-WO_3, < -43 °C), triclinic (δ-WO_3, -43 *to* 17 °C), monoclinic I (γ-WO_3, <17 *to* 330 °C), orthorhombic (β-WO_3, <330 *to* 740 °C), tetragonal (α-WO_3, >740 °C) [35–38]. The monoclinic γ-WO_3 phase with the $P2_1/c$ (or $P2_1/n$) space group, which comprises a primitive monoclinic unit cell, a two-fold screw axis, and a c-glide plane perpendicular to the screw axis (Table 1) [35].

WO_3 can be also encountered in a non-stoichiometric structure, WO_{3-x} (where $0 < x \leq 1$); however, WO_{3+x} seldomly occurs in nature [39]. The wide variability of these nonstoichiometric structures stems from the WO_x lattice, which can withstand a considerable number of O

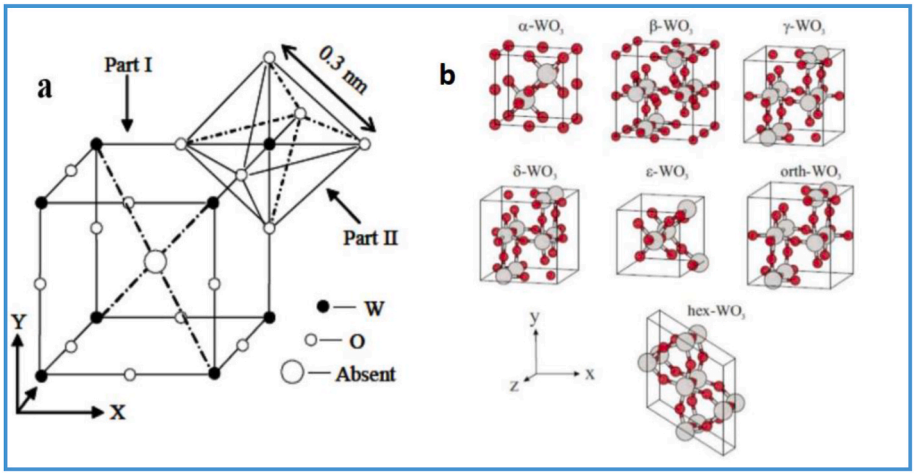

Fig. 7. (a) Geometry of the ReO_3-type unit-cell at the [WO_6] octahedral site; (b) Unit cells of different (WO_x) phases [34].

Table 1
Unit-cell parameters and densities of the different WO_3 phases.

Crystal	Space Group	a	b	c (Å)	α	β	γ(°)	ρ (g/cm^3)
ε-WO_3	*Pc*	5.278	5.156	7.664	90	90.76	90	7.39
δ-WO_3	P-1	7.313	7.525	7.689	88.85	90.91	90.94	7.28
γ-WO_3	$P2_1/c$	7.306	7.540	7.692	90	90.88	90	7.27
β-WO_3	Pmnb	7.341	7.570	7.754	90	90	90	7.15
α-WO_3	*P4/nmm*	5.272	5.272	3.920	90	90	90	7.07
Cubic WO_3	Pm-3m	3.834	3.834	3.834	90	90	90	6.83
h-WO_3	*P6/mmm*	7.298	7.298	3.899	90	90	120	6.42

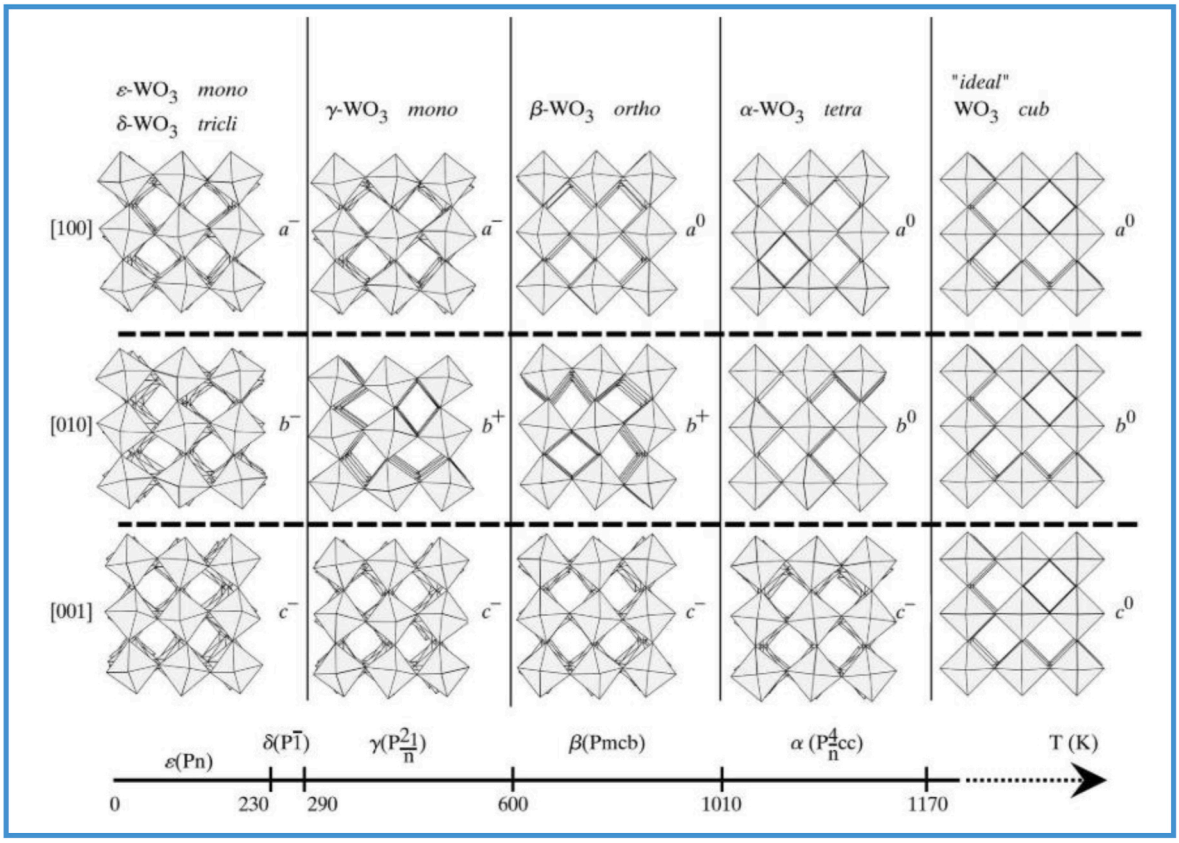

Fig. 8. Tilt patterns and stability temperature domains of the different WO_3 polymorphs [38].

deficiencies, resulting in the formation of different oxidation states for W. WO_x can vary from $WO_{2.625}$ ($W_{32}O_{84}$) to $WO_{2.96}$, and can be identified by the local condensation associated with the edge-sharing octahedral site organisation, which in turn arises from the pure corner-sharing networks of the WO_6 octahedra in stoichiometric WO_3 [39].

2.1.2. Electronic band structure and optical properties of WO_x

As shown in Fig. 9, WO_3 exhibits an electronic bandgap corresponding to the energy difference between the valence band, which is occupied with the electrons originating from the O 2p orbitals, and the conduction band, which is mainly formed by empty W 5d orbitals [40]. The conduction band primarily consists of t_{2g} orbitals ($5d_{xy}$, $5d_{yz}$, and $5d_{xz}$), whereas the e_g orbitals ($d_{x^2-y^2}$, d_{z^2}) are located at much higher energies. Notably, WO_{3-x} ($x < 1$) manifests with an additional narrow band of electronically occupied states directly below the CB. The accurate energy levels of the excess electrons in the orbitals with d-symmetry in the CB depend on whether the vacancies are created in the direction of the -W-O-W- chain [32].

The WO_3 allotropic forms also exhibit changes in terms of bandgap energy, as the occupied levels of the W 5d states slightly change with the phase transformations. Amorphous WO_3 typically possesses a relatively large bandgap energy of approximately 3.25 eV, whereas the respective bandgap energy of monoclinic WO_3 in bulk form (large crystallite size) is ~2.6 eV [41].

Moreover, in nanostructured WO_3, the reduction in crystallite size results in a blue shift of the optical absorption band edge, corresponding to a widening of the bandgap energy, with reported values ranging from 2.60 to 3.52 eV. The largest blue shift can be theoretically attributed to the quantum confinement effect [42]. Since the colour of WO_3 is mainly determined by the absorption edge energy of the material, its monoclinic form is usually yellowish, whereas its nanoparticles are white. The oxygen-deficient WO_x phases are typically light blue or green, which is caused by an additional absorption phenomenon due to the electron transfer from W^{6+} to W^{5+}. It is also important to mention that WO_3 is characterised by a high refractive index, ranging from 2 to 2.5, which is ideal for the design of WO_3-based optical devices [43].

2.1.3. Photochromism in WO_x-based materials

Hitherto, various theoretical models have been proposed to elucidate the photochromism mechanisms of WO_3. In the two earliest models, Deb et al. proposed that photochromism is induced by F-centre-like absorptions between the ground and excited states of electrons trapped in oxygen vacancies, whereas Leiderer et al. hypothesised that the light-induced decomposition of H_2O generates the formation of protons (H^+) and metastable oxygen radicals, leading to the stabilisation of W^{5+} ions and thereby causing photochromism [44,45]. Indeed, the protons and optically excited electrons lead to the formation of coloured tungsten bronze HWO_3 species. Bechinger et al. noted that the manifestation of blue colouration in WO_3 films stemmed from the systematically increasing H content when protons were used as injected ions [46]. In addition, Sun et al. suggested that structural defects, such as localised impurities and dislocations, played important roles in the photochromic behaviour of WO_3 [47].

The studies discussed above highlight the intervalent electron transfer between tungsten ions with different valence states as the fundamental mechanism underlying photochromism. When WO_3-based materials are irradiated with light, electrons (e^-) and holes (h^+) are generated, and the electrons enter the conduction band of WO_3. Then, in a typical scheme described in the literature, the holes react with the adsorbed water molecules on the oxide surface to create H^+, which then diffuse into WO_3, resulting in a change in colour [45]. This process can be summarised as follows:

$$WO_3 + hv \rightarrow WO_3^* + e^- + h^+$$

$$h^+ + 1/2H2O \rightarrow 1/4O_2 + h^+$$

$$WO_3 + xe^- + xH^+ \rightarrow H_xWO_3$$

Despite the enormous number of studies discussing the mechanism of photochromism, this process is not yet fully understood. In addition, photochromism in nanocrystalline WO_3 films, or WO_3-based organic or inorganic composites, has not been thoroughly studied. The recent developments regarding WO_3-based inorganic compounds and their improved photochromism mechanism are discussed in detail below.

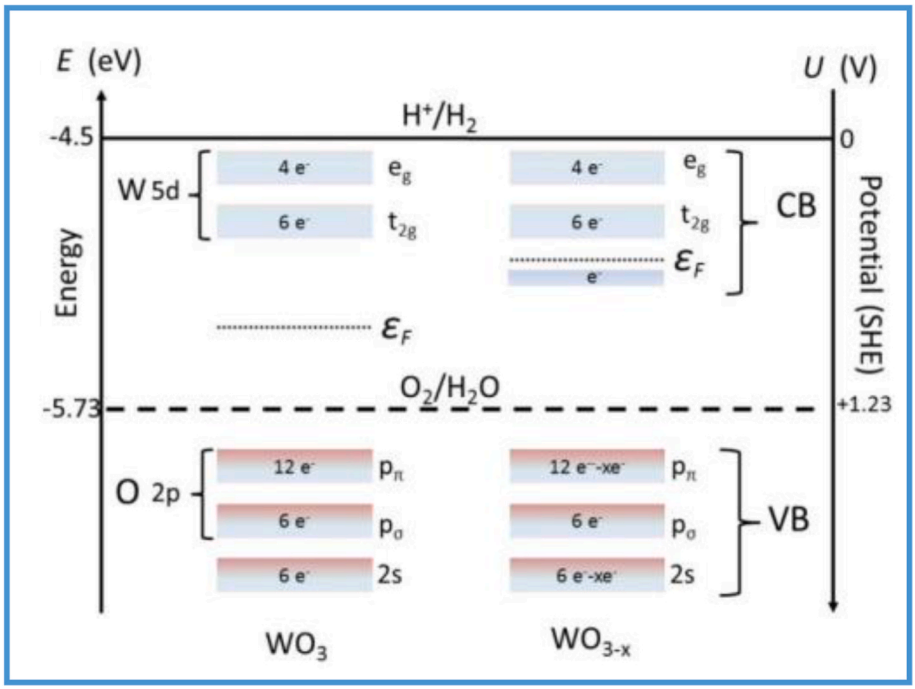

Fig. 9. The electronic band states on the y-axis in WO_3 and WO_{3-x}. To the left is the energy (eV) and to the right is the potential, according to the standard hydrogen potential (SHE) in vacuum [40].

2.1.4. Recent developments in WO_x-based inorganic materials

Although pristine WO_x-based materials exhibit good photochromic behaviour, this intrinsic property presents several restrictions, including a limited applicable wavelength range, poor reversibility, and low photoresponse amplitude [48]. With these drawbacks, expanding the research on WO_3-based photochromic materials and devices is inevitable. In this section, we report the latest improvements in photochromic WO_3-based inorganic materials and devices. Since WO_3 usually possesses poor reversibility, a small change in optical density between its coloured and bleached states, a narrow response in the spectrum, low fatigability, and slow response times [49], considerable attention has been devoted to the development of composite inorganic materials with synergistic properties and improved performance, for use in diverse applications.

2.1.5. Doping

Since WO_3 is an n-type wide-bandgap semiconductor, its photochromic transition from yellow to blue is achieved under UV irradiation below 370 nm. Doping with typical elements, such as Al, Cu, Mo, Zn, and Co, has been confirmed to be a feasible method for decreasing the bandgap of WO_3 *via* the introduction of a transition band between the CB and VB.

Very recently (2021), Dong et al. conducted a detailed study on the effect of Cu doping on the photochromic properties of WO_3 [50]. In their work, Cu@h-WO_3/WO_3·nH_2O hierarchical microsphere composites were fabricated using a hydrothermal method and modulated by modifying the doping amount of Cu. Fig. 10 shows the colour changes of the products during photochromism and self-bleaching. Pure WO changed from light yellow to light cyan after UV irradiation for 2.0 min, maintaining this colour for at least 60 min. The self-bleaching process was greatly accelerated upon increasing the Cu doping concentration, and a return to the original colour could be achieved within 60 min by simply keeping the materials in the dark, without the need for additional treatment. As shown in Fig. 10, the photogenerated electrons excited from the h-WO_3 VB after UV irradiation were partly trapped by Cu^{2+} cations during their migration to the WO_3 surface, caused by interfacial charge transfer (IFCT), resulting in the efficient separation of photo-induced electron-hole pairs. W^{6+} and Cu^{2+} were reduced to W^{5+}, Cu^{+}, and Cu^{0}, respectively. The generated protons were subsequently inserted into the lattice along the open channels and then interacted with the elongated W–O chains to form hydrogen tungsten bronze ($H_xW^{VI}_{1-x}W_x^{V}O_3$).

The effect of Mo doping on the photochromic behaviour of WO_3-based composite films was studied by Miyazaki et al., who fabricated composite films using a transparent urethane resin matrix [51]. Fig. 11 shows the transmittance spectra of the composite films obtained before and after ultraviolet–visible (UV–vis) light irradiation, where the absorption peak positions can be observed to shift to lower wavelengths (blue shift) with an increase in the Mo/W ratio. In addition, the reaction rate constants of the Mo-doped films were larger than those of the non-doped films, confirming the enhanced photochromic reversibility of the former.

Avellaneda et al. investigated the influence of Nb, Ta, Ti, and Zr doping on the photochromic properties of doped-WO_3 films prepared *via* dip coating on a glass substrate [52]. The differences between the coloured and photobleached state responses for the doped and undoped WO_3 films were measured in the wavelength range of 300–2100 nm at various temperatures: 25, 100, 120, and 150 °C. The best photochromic response was reported for the WO_3:Zr films, for which $\Delta T = 59.35\%$ (435 nm, at 100 °C).

The photochromic behaviour was highly improved by Al^{3+} doping, as reported by Shen et al. [53]. Al-doped WO_3 powder with significantly enhanced structural, morphological, and photochromic properties was successfully synthesised using a hydrothermal route at low temperature. Moreover, the colour contrast (ΔC) of all WO_3 samples was calculated before and after UV irradiation (365 nm, 5 min), where the photochromic activity of the Al-doped WO_3 samples was revealed to increase along with the increasing Al^{3+} doping concentration, reaching a maximum at a molar concentration of 0.25%, beyond which photo-activity began to decrease. This behaviour was attributed to the escalating recombination of electron/hole pairs as the concentration of local defects became too high.

Photocatalytic activity, which can be considered as a property directly linked to the photochromism of pure, as well as Zn, Cu, Zn, and Cu co-doped WO_3 nanoparticle samples was studied by Mohammadi et al. under UV–vis light irradiation [54]. The as-prepared nanoparticles, with sizes about 20–30 nm (Fig. 12), exhibited smart optical properties with bandgaps ranging from 2.97 to 3.20 eV, depending on the doping element. The results showed that the Zn and Cu co-doped WO_3 nanoparticles possessed the highest photocatalytic activities, while the red shift of the absorption edge and the improvement of the charge carrier trapping effect were ascribed to the effects of doping.

2.2. Other photochromic TMOs

The optical and electronic properties of TiO_2, V_2O_5, and MoO_3 depend on the oxygen vacancies concentration, and can therefore be modified by adjusting this feature. These three inorganic oxides, which

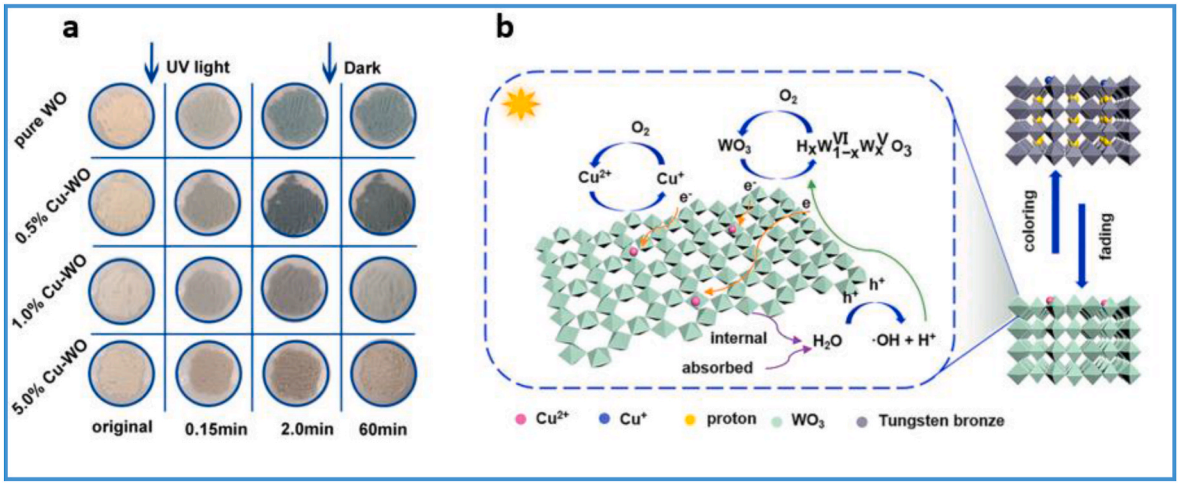

Fig. 10. (a) Photos of samples after photochromism and self-bleaching; (b) Schematic diagram of the photochromic mechanism in Cu@h-WO_3/WO_3·nH_2O hierarchical microspheres [50].

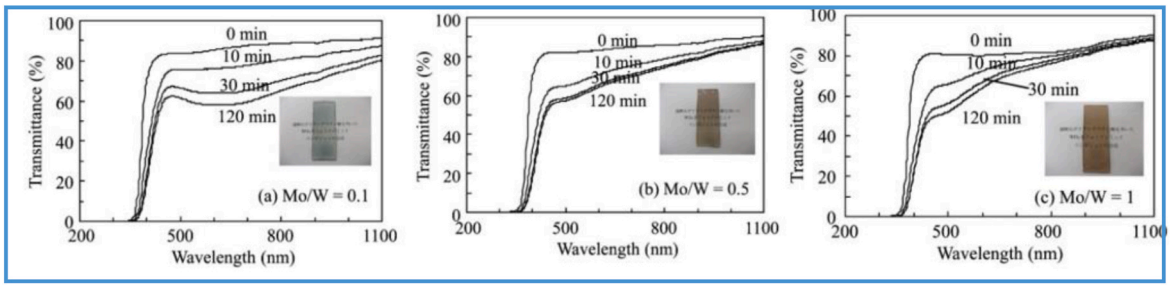

Fig. 11. (Colour online) Transmittance spectra of composite films with various Mo/W ratios before and after UV–vis light irradiation. Inset photographs in respective graphs show the films after 120 min of UV–vis irradiation [51]. (For interpretation of the references to colour in this figure legend, the reader is referred to the Web version of this article.)

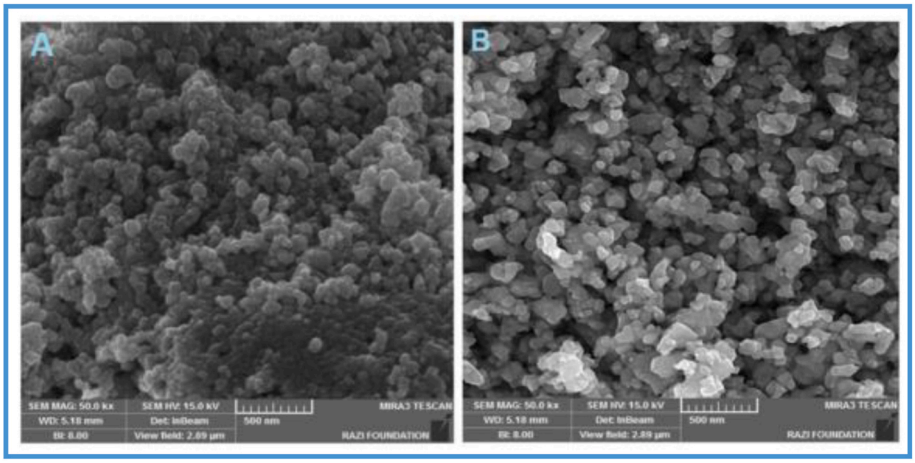

Fig. 12. FE-SEM images of (a) pure and (b) Zn/Cu co-doped WO_3 nanoparticles [54].

share the $ns^0(n\text{-}1)d^0$ electronic configuration, are wide-bandgap semiconductors based on transition metals with higher oxidation states, namely Ti^{4+}, V^{5+}, and Mo^{6+}. In general, photochromism is achieved *via* the photoredox catalysis of a small fraction of M^{n+} to $M^{(n-1)+}$ ions: Ti^{3+}, V^{4+}, and Mo^{5+}, respectively.

2.2.1. Molybdenum oxide (MoO_3)

Molybdenum VI trioxide (MoO_3) is an interesting wide-band-gap n-type TMO because it can form several allotropes, all comprising MoO_6 octahedra as the basic structural element, but with varying oxygen vacancy contents [55]. Commercial MoO_3 is available in the form of white or light grey powder.

Orthorhombic molybdenum trioxide (α-MoO_3), one of the most popular photochromic inorganic materials, consists of dual-layer planar crystals of distorted MoO_6 octahedra held together in the vertical direction by weak van der Waals forces [56]. The electrons in the oxygen 2p orbitals can be reversibly excited to the molybdenum 4d orbitals, resulting in the valence state change of molybdenum from Mo^{6+} to Mo^{5+}, which leads to blue colouration [57]. Different strategies have been implemented to improve the photochromism of MoO_3, such as modifying with noble metals (*e.g.*, Au, Pt), accelerating the separation of electron-hole pairs, combining with other metal oxides (such as WO_3, through Mo-to-W transition), intercalation of zerovalent metals, and engineering to nanostructures or metastable structures [57–60]. Rao et al. reported the use of a cadmium sulfide (CdS) interlayer in a MoO_3/CdS system, where electrons were injected from the CdS semiconductor to the oxide film by taking advantage of the lower bandgap energy of CdS (~2.4 eV) compared to that of MoO_3 (≥3.0 eV) [61]. In another study, Tomás et al. deposited ZnSe–MoO_3 thin films on glass substrates *via* thermal evaporation of a MoO_3–ZnSe powder mixture [62]. Compared with the undoped MoO_3 films, the 5 mol% ZnSe-doped films exhibited better photochromic and thermochromic responses, although the latter property was improved only for temperatures below 125 °C (Fig. 13).

2.2.2. Vanadium pentoxide (V_2O_5)

Vanadium exists in several oxide forms, such as di-, sesqui-, and pentoxide (VO_2, V_2O_3, and V_2O_5, respectively), which have all been processed in thin film forms and applied as optical and electrical devices. In particular, V_2O_5 has been widely investigated as a wide-bandgap n-type semiconductor in regard to its photochromic properties, apart from numerous other applications including cathodes in electrochromic devices, electronic information displays, colour memory devices, and micro batteries [63,64].

In 2002, Nishio et al. demonstrated for the first time the visible-light photochromism features of polycrystalline V_2O_5 [65]. The oxide turned blue-black upon irradiation with visible laser light (514.5 nm) in an air environment, stemming from the photoreduction of V^{5+}. This effect was confirmed to be entirely irradiation-induced, as the blue-black colouration was completely reversed by subsequent heating at 400 °C for 10 min (Fig. 14). More importantly, the colour change could be induced in the same region of the material without significant degradation of the photochromic performance (as indicated by photoluminescence measurements), thus demonstrating its good cyclability.

2.2.3. Titanium oxide (TiO_2)

TiO_2 is a chemically stable, nontoxic, biocompatible, and inexpensive material with a very high dielectric constant and interesting photochromic properties [66]; however, its wide bandgap can often hinder the efficiency of TiO_2-based nanomaterials. The bandgap of bulk TiO_2 lies in the UV regime (3.0 and 3.2 eV for the rutile and anatase phases, respectively), which is only a small fraction of the sun's energy

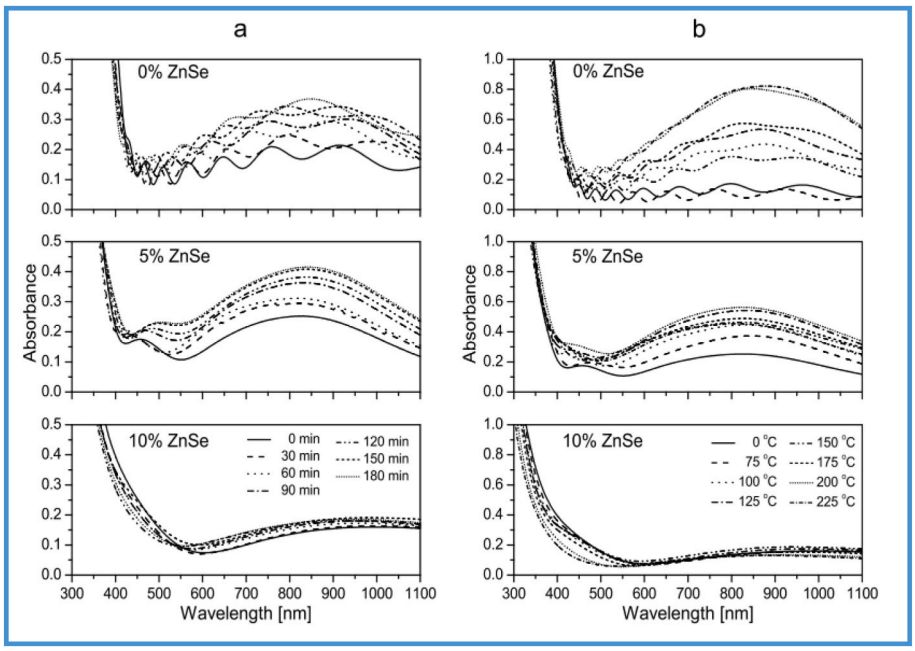

Fig. 13. Optical absorption spectra of the (a) irradiated and (b) annealed ZnSe-doped MoO_3 films [62].

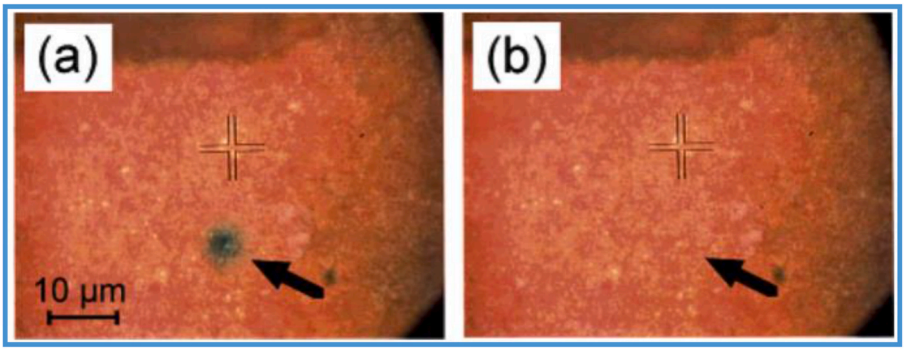

Fig. 14. Optical micrographs of polycrystalline V_2O_5 after (a) irradiation for 60 min and (b) subsequent heating at 400 °C for 10 min. Target area is indicated by the arrow [65].

(<10%) [67]. Thus, a primary concern for improving the performance of TiO_2 nanomaterials is increasing their optical activity by shifting their response onset from the UV to the visible region. There are several ways to achieve this goal, such as doping TiO_2 nanomaterials with other elements or sensitising them to visible light using colourful inorganic/organic compounds [68].

Daniel et al. examined thin films consisting of a TiO_2-silver nanoparticle composite, showing that under an Ag content larger than 50 mol %, good visible light-responsive properties were obtained [69].

In another recent study by Naoi et al., Ag–TiO_2 films were prepared by the photoelectrochemical reduction of Ag^+ to Ag nanoparticles in nanoporous TiO_2 films, under UV irradiation [70]. These films changed from brownish grey to light beige under exposure to coloured visible light, and reverted to their initial colour under UV irradiation. In addition, the authors were able to control the photochromic behaviour and chromogenic properties by regulating the irradiation conditions, as well as the geometry and matrix of the nanopores (Fig. 15). The chromogenic properties of these composite films were improved *via* simultaneous irradiation with UV and blue light, which suppressed the formation of anisotropic Ag particles that are known to obstruct photochromism.

In 2018, Valden et al. synthesised quantum dots by dispersing irregularly shaped anatase TiO_2 nanoparticles (NPs) in butanol (8 wt%) [71], successfully achieving photochromic functionality. They demonstrated that the transmittance of the NPs can be strongly modulated over a wide optical range (from 400 to 12,000 nm) and identified two distinct physical mechanisms that explained the observed phenomena: first, light exposure generated polaronic lattice distortions in the NPs, thus inducing transmittance in the visible region of the spectrum. Second, the absorption mechanism originating from the photoreduction of TiO_2 during UV irradiation, caused photochromism to manifest in the IR region of the spectrum. Although the photoreduction of TiO_2 led to the formation of Ti^{3+}, only a small fraction of the photogenerated electrons were trapped in this form (approximately 0.5%). As such, the majority of photogenerated electrons remained as free charge carriers.

2.3. *Photochromism on Schottky barriers at inorganic composite interfaces*

The preceding part clearly established that the majority of inorganic photochromic compounds are based on the photoreduction of the metallic element in wide-bandgap semiconductors, such as MoO_3, WO_3, TiO_2, V_2O_5, or Nb_2O_5. Despite the unique properties and contribution of WO_3 (in terms of its synthetic methods history, crystallite size, oxygen/tungsten stoichiometry, *etc.*) having been extensively discussed, the mechanisms governing the photochromic effect in such transition metal

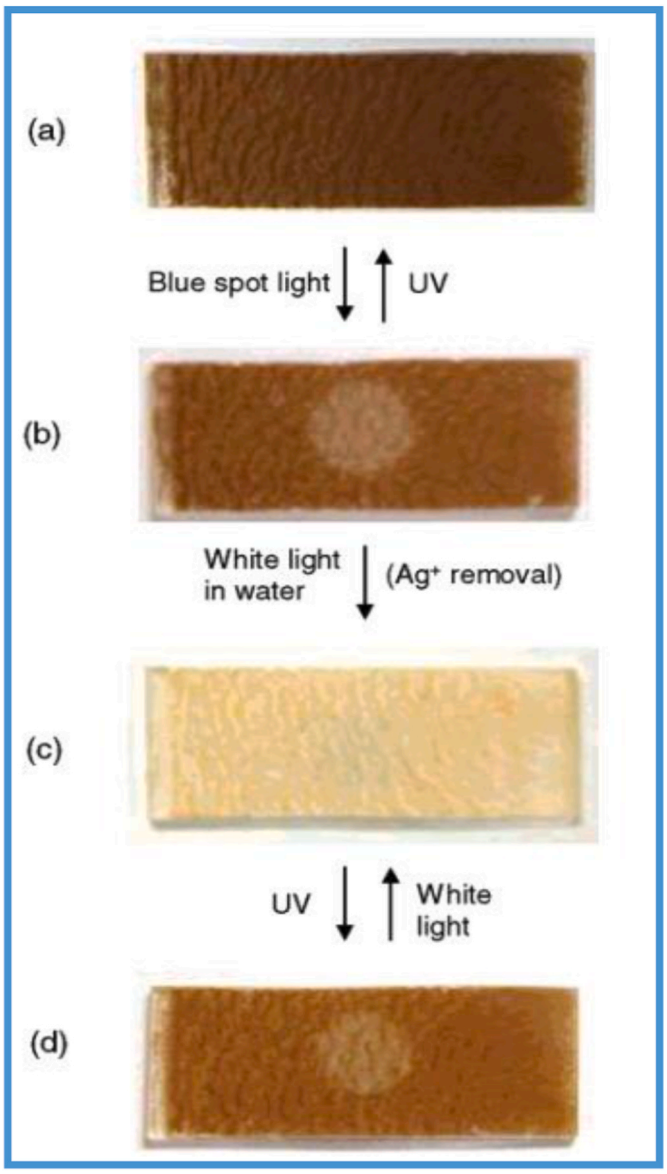

Fig. 15. (a) Pristine TiO_2 film loaded with Ag nanoparticles (brownish grey). (b) The film irradiated with a blue spot light (450 nm; fwhm, 10 nm; 2 mW cm^{-2}; 60 min; diameter: 6 mm). (c) Subsequent irradiation with white light (50 mW cm^{-2}, 6 h). (d) The film was further irradiated with UV light (310 nm, 0.1 mW cm^{-2}, 15 min) [70]. (For interpretation of the references to colour in this figure legend, the reader is referred to the Web version of this article.)

oxides are not yet fully understood and still remain subject to debate, even sparking a few controversies. However, it is widely accepted that photochromism is induced by irradiation at specific wavelengths which allow electron transfer across the semiconductor forbidden bandgap, where electrons from the VB have enough energy to be excited to the CB, thus creating exciton pairs. In pristine transition metal oxides, charge depletion can then occur when atmospheric water is "oxidised" by the VB holes [72]. Protons can thus be integrated into the crystal structure (bronze creation) and trap the remaining unpaired electrons, leading to the reduced metallic species W^{5+} in WO_3, Mo^{5+} in MoO_3, V^{4+} in V_2O_5, *etc*. In general, the blue colour results from the intervalence charge transfer (IVCT) typically occurring between the $TMO^{(n-1)+}$ defects and TMO^{n+} species, which produces absorption on the border between the visible and near-infrared parts of the spectrum.

Two recent reviews by Wang et al. and He et al. (Fig. 16) have demonstrated the benefits of establishing a Schottky interface with a second compound in WO_3-based photochromic materials [73,74]. Their works again highlighted the strongest limitation of WO_3 photochromic materials, namely, their negligible reversibility, or ability to recover the photobleached state only *via* oxidative treatments. Thus, these reviews have verified that the photochromic efficiency of inorganic oxides can be effectively enhanced when combining them with other organic or inorganic materials. This discovery has led to the creation of solid-solid interfaces, which can be described as Schottky barriers. A substantial improvement in the charge depletion rate can be realised in such interfaces (*i.e.*, spatial separation of the holes and electrons created by irradiation), thus promoting the photoredox reactions occurring at the start of photochromism. The most interesting aspect is that charge depletion is not associated with chemical TMO transformation and the introduction of protons, therefore allowing for the reversibility of the photochromic phenomenon (*i.e.*, self-reversibility without the use of heat treatment or an oxidative atmosphere). In view of these discoveries, numerous novel composite or mixed oxide materials with improved multicolour and reversible photochromism performance, visible-light colouration properties, and fast photo response have been prepared during the last two decades.

Numerous studies have confirmed that using a photochromic TMO (such as MoO_3) alone does not yield satisfying photochromic contrast, whereas its combination with gold or platinum nanoparticles, and the subsequent formation of Schottky barriers, leads to a drastic improvement in the overall photochromic performance [75–78]. This effect can be evidenced in the solar transmittance contrast between thin composite films in their photobleached and coloured states, as well as the extension of their light response from UV radiation to visible sunlight. The enhancement in the visible-light photochromism of MoO_3/Au or MoO_3/Pt thin-films can be explained by the electrons capture by Au and Pt, which results in a longer electron-hole pair separation time, analogous to the photocatalytic enhancement effect when Pt or Au metals are deposited on inorganic semiconductor surfaces [79,80].

Fig. 17 illustrates the main discoveries of Zhao et al. [82]. The authors have established Schottky barriers between a metal and MoO_3, achieving an increase in the adsorbed water on the MoO_3 film surface (films are prepared by vacuum evaporation), which in turn enhances the utilisation of the photogenerated holes during the colouration process, and thus facilitates the separation of photogenerated carriers. As a result, the photochromic performance of the MoO_3/Au film was significantly enhanced compared to that of the pristine MoO_3 films, achieved from the accelerated electron-hole transfer at the Schottky barrier. In a similar study by Yao et al., however, no information regarding the exact surface power received by the samples from the UV irradiation source is available. In addition, the reversibility of the photochromic films was not further studied.

Parallelly, some authors have demonstrated that the generation of colour centres (Mo^{5+} and/or Mo^{4+} ionic species) in MoO_3 thin films under UV light absorption is more effective when these films are coated on CdS glass substrates [81,82]. This phenomenon is ascribed to the formation of Schottky barriers at the interface between the two inorganic semiconductors. Similarly, the combination of WO_3 and CdS also leads to enhanced photochromic activity [82].

It should be noted, however, that the first set of publications related to Schottky barrier creation, *ca.* 2000, suffered from a lack of understanding of the Schottky mechanism. Furthermore, the inability to chemically modify the TMOs (control of the oxygen stoichiometry, structural form, *etc.*) with the aim of tuning the optical contrast between the coloured and photobleached states, as well as the kinetics of the colouration process and the reversibility of the photochromism mechanism, is a critical limitation.

The strategy of combining TMOs with other metal oxides to improve photochromism was recently explored by proposing various composite powder/films, including MoO_3-WO_3, ZnO-WO_3, TiO_2-WO_3, TiO_2–MoO_3, *etc*., or even crystalline-amorphous WO_3-WO_{3-x} particles with abundant proton sources and rich oxygen vacancies in the homojunctions [83–92].

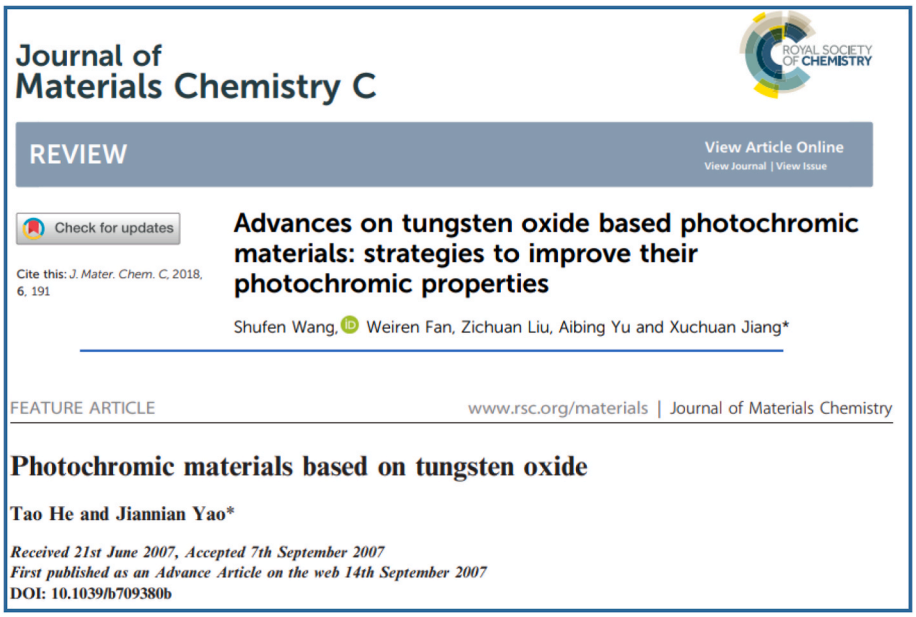
Journal of Materials Chemistry C

REVIEW

View Article Online
View Journal | View Issue

Check for updates

Cite this: J. Mater. Chem. C, 2018, 6, 191

Advances on tungsten oxide based photochromic materials: strategies to improve their photochromic properties

Shufen Wang, Weiren Fan, Zichuan Liu, Aibing Yu and Xuchuan Jiang*

FEATURE ARTICLE www.rsc.org/materials | Journal of Materials Chemistry

Photochromic materials based on tungsten oxide

Tao He and Jiannian Yao*

Received 21st June 2007, Accepted 7th September 2007
First published as an Advance Article on the web 14th September 2007
DOI: 10.1039/b709380b

Fig. 16. Front pages of the reviews of Wang et al. and He et al.

This new set of studies, taking place in the 2010s, has taken advantage of new synthetic routes, allowing the construction of complex nanoparticle (NP) architectures. As a representative example, ZnO NP-functionalised WO_3 vertical plate-like arrays were synthesised and characterised by Li et al., using a combination of hydrothermal and electrodeposition methods [92]. The experimental results indicated that the ZnO NP-functionalised WO_3 arrays produced a higher photocurrent under visible light irradiation, which was attributed to the effective transfer of the photogenerated holes, which in turn retarded the recombination of electrons and holes at the oxide/oxide interfaces (Fig. 18). As another example, Ahmed et al. deposited MoO_3-WO_3 films with different compositions on glass substrates *via* laser powder deposition (LPD) [85]. The deposited films were annealed at different temperatures and characterised in terms of their photochromic properties. The UV–vis transmittance spectra revealed that the mixed oxide films were less transparent when compared with pure MoO_3 films (Fig. 19). However, the intensity of the blue colour of the composite film increased along with the increasing irradiation time.

In 2019, Oderinde et al. synthesised a WO_3/MoO_3 oxide composite using the deep eutectic solvent (DES) ethaline [94]. The as-prepared composite consisted of nanosized cuboctahedra-like crystals, indicating that DESs could be used to fabricate nanocrystals at low temperatures. Furthermore, the photochromic response of the as-prepared composite was observed under visible light irradiation. Fig. 20a shows photographs of the as-prepared composite samples before and during irradiation, and their reverse colouration. The studied sample was cream-yellow in colour before irradiation, but became blue after 5 s of radiation exposure, with the colour intensity increasing along with the increasing exposure time. The reflectance percentage in the visible light region dramatically decreased in intensity as the UV irradiation time increased, becoming fully saturated after 60 s (Fig. 20b). The photochromism behaviour of the composite was attributed to the optical absorption band originating from the light-induced intervalence electron transfer between neighbouring W/Mo cations, which was explained according to the intervalence electron transfer model, as Mo and W sites were involved in the redox process in the mixed oxides due to the different valence states (W^{6+}, W^{5+}, W^{4+}, Mo^{6+}, Mo^{5+}, Mo^{4+}) or different structural surroundings (Fig. 20c) [95]. The electron transfer (ET) mechanism was also related to photoinduced processes, such as charge transfer (or electron donor-acceptor), at the MoO_3/WO_3 interface. In addition, the reflectance intensity was maintained almost exactly after 15 colouration-bleaching cycles (Fig. 20d), demonstrating an almost complete reversibility of the cream-yellow to deep-blue colour switching process.

In order to achieve faster photobleaching, reduced graphene oxide (rGO)-doped tungsten trioxide/molybdenum trioxide (WO_3/MoO_3) composite powders (with different rGO concentrations) were recently prepared *via* a simple co-precipitation method by Lek et al. [96]. The colouration and bleaching processes were studied in accordance with the colour difference ΔC of the film before and after irradiation with UV light for 50 min (Fig. 21). The ΔC of the films decreased as the RGO content increased, due to the dark colour of the latter. Therefore, the ΔC before and after irradiation was less than that of the undoped RGO film, whereas WO_3/MoO_3 exhibited the greatest ΔC, which changed from white to dark blue after 50 min of UV irradiation. Fig. 21 shows a coloured photograph of the films that were exposed to UV radiation for 50 min and then thermally treated at 80 °C for 20 and 360 min. Under UV irradiation, the colour of the WO_3/MoO_3 film changed from white to dark blue, whereas the RGO-doped WO_3/MoO_3 films changed from grey to dark blue. The WO_3/MoO_3 composite materials exhibited enhanced photochromic performance, as compared to those of pure WO_3 or MoO_3, because the electrons in mixed oxide composite materials transfer from Mo^{5+} to W^{6+} (Mo → W), assuming that the MoO_3 work function was higher than that of WO_3. The improvement in the reversibility of the photochromic properties was due to RGO having a charge-carrier mobility of 20,000 cm^2/V, resulting in an increase in the charge separation efficiency. During irradiation, the photogenerated electrons were continuously transferred through RGO from the CB of WO_3 to the CB of MoO_3. Accordingly, holes transferred from the VB of MoO_3 to the VB of WO_3. Electrons were trapped at the CB of MoO_3 and holes were trapped in the VB of WO_3, both of which migrated by electron-reduced water to H^+ and holes-oxidised water to O_2, forming hydrogen bronze (blue colour).

Among semiconductor materials, TiO_2 has attracted significant attention because of its favourable chemical and physical properties, low cost, high stability, and positive influence on the photochromism of WO_3 [97]. He et al. prepared WO_3 and TiO_2 colloids using a forced hydrolysis technique [98]. Fig. 22 shows the UV–vis absorption spectra of the (a) WO_3 and (b) WO_3/TiO_2 colloids. Prior to UV irradiation both films were almost transparent, but when irradiated with UV light for 3 min, they turned deep blue, and a broad absorption peak at approximately 900 nm appeared in their spectrum. These results indicated that

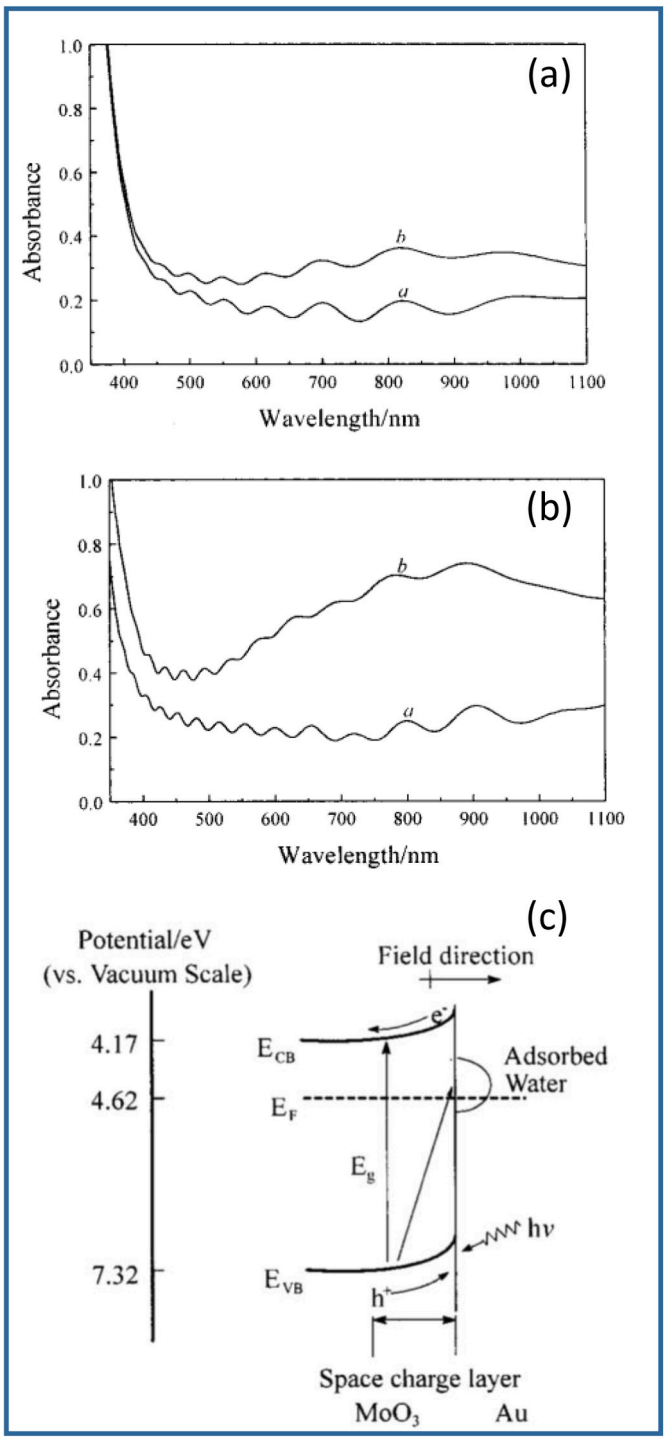

Fig. 17. Absorption spectra of vacuum-evaporated thin films of (a) MoO_3 and (b) MoO_3/Au: (curve a) as-prepared films and (curve b) spectra taken after UV irradiation for 3 min in air. (c) Schematic diagram for the Schottky barrier and the charge-transfer process at the MoO_3/Au interface [82].

the UV radiation-induced colouration of WO_3 colloids can be greatly improved by combining with TiO_2. In addition, Yao et al. proposed an enhancement mechanism, relying on the generation of electrons and holes in the WO_3 or TiO_2 colloids under UV irradiation (Fig. 22). In this mechanism, some of the positive holes created in the WO_3 particles migrate to the valence band of TiO_2 particles, owing to the more positive potential of the former's valence band. Parallelly, since the electrons at higher energy levels tend to collapse to lower energy levels, most of the electrons created in the WO_3 and TiO_2 particles will ultimately transfer to the energy level with the most positive potential (0.85 V in WO_3). As such, the electrons and holes originally generated in either WO_3 or TiO_2 are efficiently separated, and their recombination is suppressed from the presence of TiO_2. As a result, more electrons are trapped in the band gap of WO_3 and contribute to the colouration process. Overall, in composite systems there are additional photogenerated electrons contributing to the colouration process, thereby leading to improved photochromism.

The application of rGO in WO_3/TiO_2 composites was also reported by Prabhu et al., who used a simple hydrothermal method [99]. Under solar light irradiation, the transparent rGO-TiO_2/WO_3 composite coatings displayed high photochromic properties, as shown in Fig. 23. The enhanced efficiency of the composites was attributed to the presence of reduced graphene oxide (rGO). The photochromic mechanism in this work was based on the model of double insertion/extraction of ions and electrons, which was developed to explain the electrochromism of WO_3 [100]. The photochromism of the rGO-TiO_2-WO_3 composites is explained as follows and illustrated in Fig. 24:

$$rGO - TiO_2WO_3 + hv \rightarrow e^- + h^+$$

$$W^{6+} + e^- \rightarrow W^{5+}$$

$$h^+ + 1/2H2O \rightarrow 1/4O_2 + h^+$$

$$WO_3 + xe^- + xH^+ \rightarrow H_xWO_3$$

During irradiation, e^--h^+ pairs are generated. The photogenerated e^- will reduce the W^{6+} oxidation state of WO_3 present in the rGO-TiO_2-WO_3 composites to W^{5+}. In contrast, the photogenerated holes react with the adsorbed water molecules, producing protons. Subsequently, the produced protons diffuse into the WO_3 lattice, resulting in the formation of H_xWO_3. The transition of electrons from the VB of W^{5+} to the CB of W^{6+} induces the blue colouration of the surface [101].

In 2019, Li et al. conducted another breakthrough research on photochromism using a self-coated WO_3/WO_{3-x} homojunction, achieving enhanced solar modulation efficiency, increased luminous transmittance, and rapid self-photobleaching rate [92]. Furthermore, for the first time, the cycling performance, reversibility, and kinetics of photochromism were thoroughly investigated. Initially, Self-coated crystalline-amorphous WO_3@WO_{3-x} nanoparticles were prepared by a simple hydrothermal method, using ammonium tungstate and oxalic acid. To prepare a 0.5-wt.% homogeneous suspension, the nanoparticles were dispersed into a water solution and stirred for approximately 1 h. Then, a transmittance analysis through the irradiation of these suspensions was performed, for quantifying their photochromic properties (Fig. 24). In conclusion, the authors stated that stemming from the abundant proton sources and rich oxygen vacancies in the homojunction, the crystalline-amorphous WO_3@WO_{3-x} nanoparticles exhibited a remarkable solar modulation efficiency and excellent luminous transmittance after colouration.

The authors asserted that their work provides a remarkable structure with robust photochromic modulation capabilities, fast bleaching rate, and good stability, which is highly attractive for smart window applications. Nonetheless, using oxalic acid as a dispersant is mandatory for obtaining such exceptional photochromic properties. Furthermore, the provision of protons, which are key particles for photochromic compounds, is also regarded as another factor hindering further development. Indeed, an effective effort to achieve the properties discussed above on water-based suspensions and window films, remains to be performed.

ZnO semiconductors have also been used to improve the chromic properties of WO_3. Recently, S.-M. Lam et al. prepared WO_3–ZnO nanorod (ZnR) nanocomposites with different loadings of WO_3 by combining a hydrothermal technique with a chemical solution process [102]. In their study, they suggested a simple explanation for the charge separation mechanism observed in WO_3-ZnR (Fig. 22): when WO_3 and

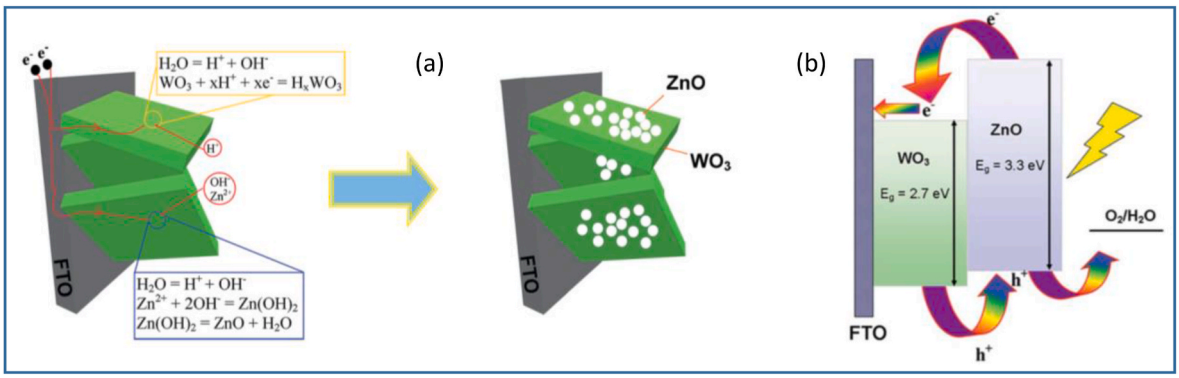

Fig. 18. Schematic illustrations of (a) the ZnO NPs-functionalised WO_3 vertical plate-like arrays synthetic process and (b) conduction and valence band positions for electron/hole transfer at the ZnO/WO_3 interface [93].

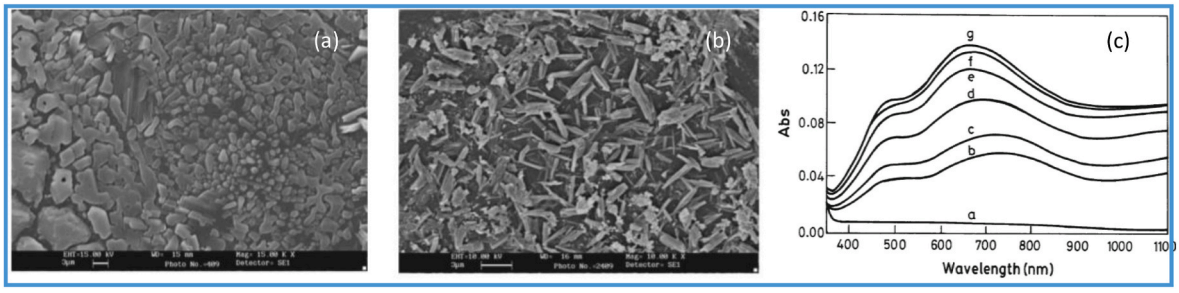

Fig. 19. SEM images of MoO_3/WO_3 composite films: (a) as deposited and (b) post-annealing treatment [85].

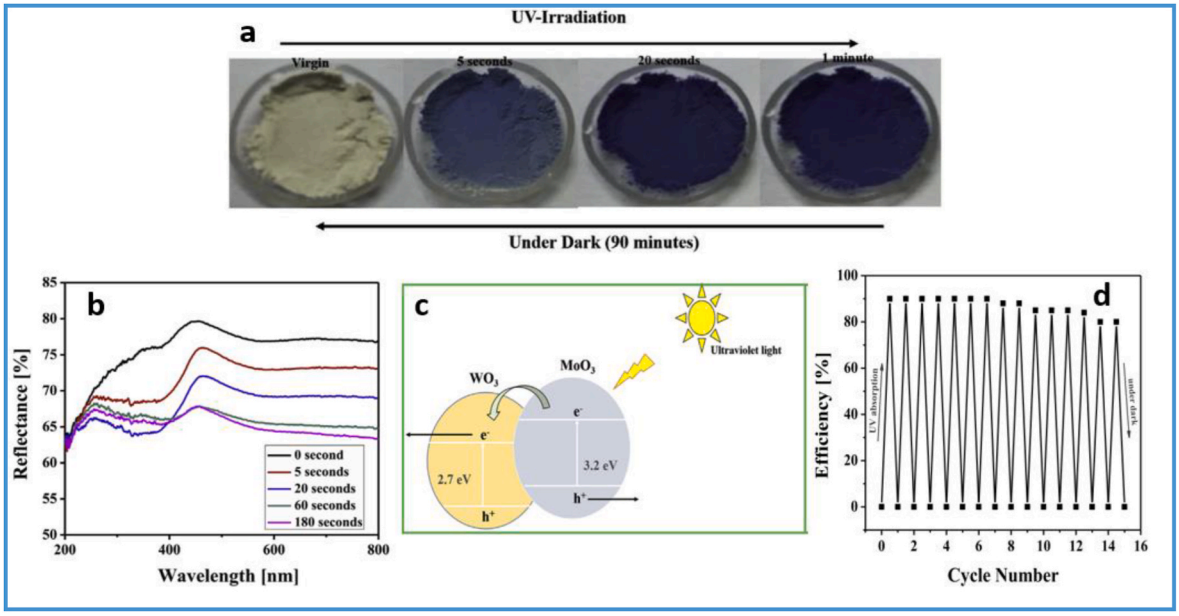

Fig. 20. (a) Photographs of the as-prepared composite MoO_3/WO_3 (10 wt% Mo) showing gradual colour change upon exposure to UV light and (b) associated UV–vis reflectance spectra. (c) Electron transfer model between neighbouring WO_3 and MoO_3 species. (d) The reflectance intensity evolution of the sample measured at 600 nm during 15 cycles [95]. (For interpretation of the references to colour in this figure legend, the reader is referred to the Web version of this article.)

ZnR form a coupled photocatalyst, upon light excitation, electrons from the valence bands of both compounds are promoted to the corresponding conduction bands, and, since the conduction band of WO_3 is lower than that of ZnR, the photogenerated electrons from the ZnR conduction band migrate to the conduction band of WO_3 [103]. Therefore, the different energy levels between the coupled semiconductors in the WO_3-ZnR nanocomposites played a significant role in facilitating the efficient electron-hole separation at the oxide interfaces.

In 2018, Sajjad et al. fabricated ZnO/WO_3 nanocomposites with different amounts of ZnO after the hydrothermal synthesis of WO_3 [104]. These nanocomposites were discovered to be highly photosensitive under visible light and had a greater photocatalytic degradation efficiency than pure WO_3 and ZnO semiconductors. The improved photodegradation efficiency is presented in Fig. 25, which illustrates the

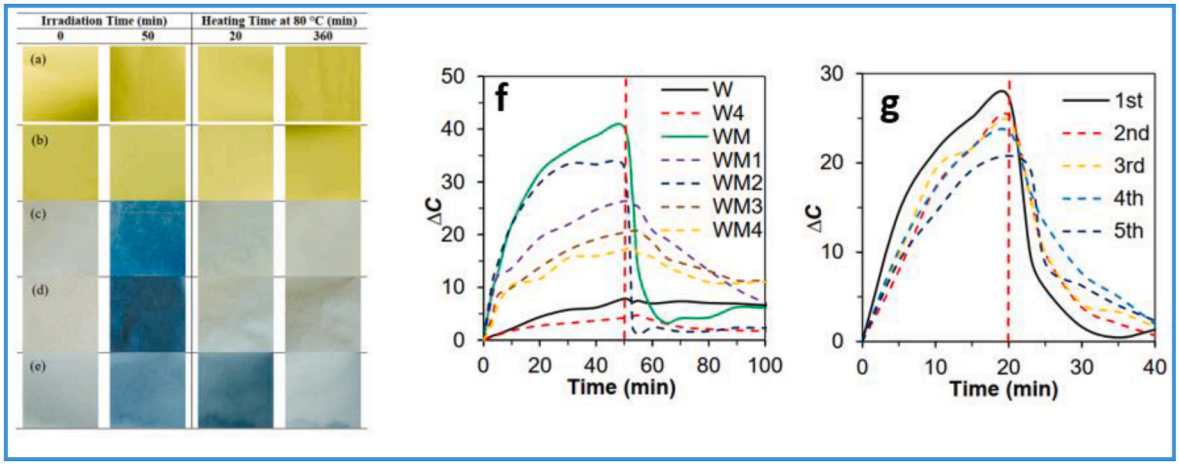

Fig. 21. Photographic images of samples: (a) W, (b) W4, (c) WM, (d) WM2, and (e) WM4 irradiated with UV light for 50 min and then kept in an oven at 80 °C f or 20 and 360 min. The colour differences (ΔC) of (f) RGO-doped WO_3 and WO_3/MoO_3 composites irradiated under UV light for 50 min and then thermally treated in an oven at 80 °C for a designated time, and (g) the stable photochromic properties of the WM2 film treated for 5 cycles [96]. (For interpretation of the references to colour in this figure legend, the reader is referred to the Web version of this article.)

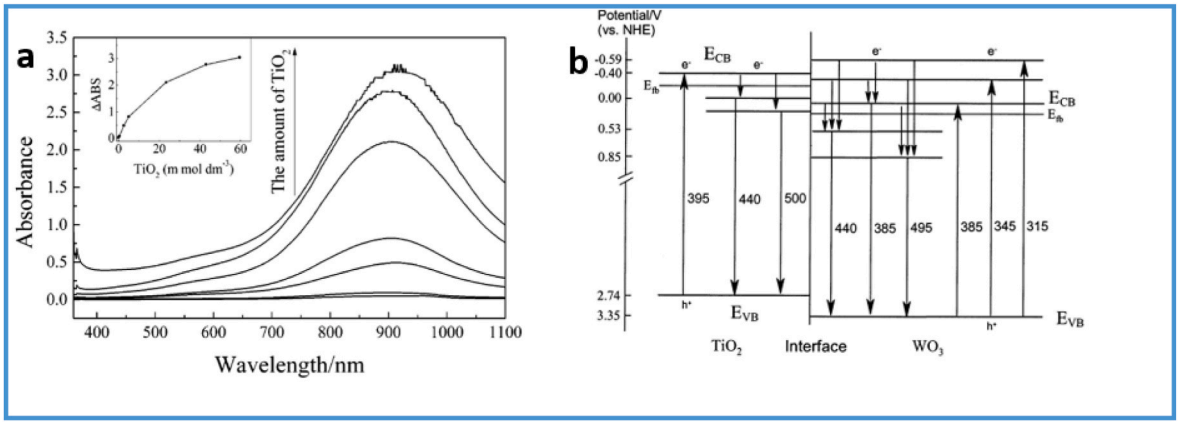

Fig. 22. (a) UV–vis spectra of the WO_3 colloids combined with TiO_2 nanoparticles at different concentrations; the pristine colloids were used as the control samples. The inset presents the dependence of ΔOD (optical density contrast) at 900 nm on the concentration of TiO_2. (b) Schematic diagram of the energy levels of the TiO_2 and WO_3 colloids [98].

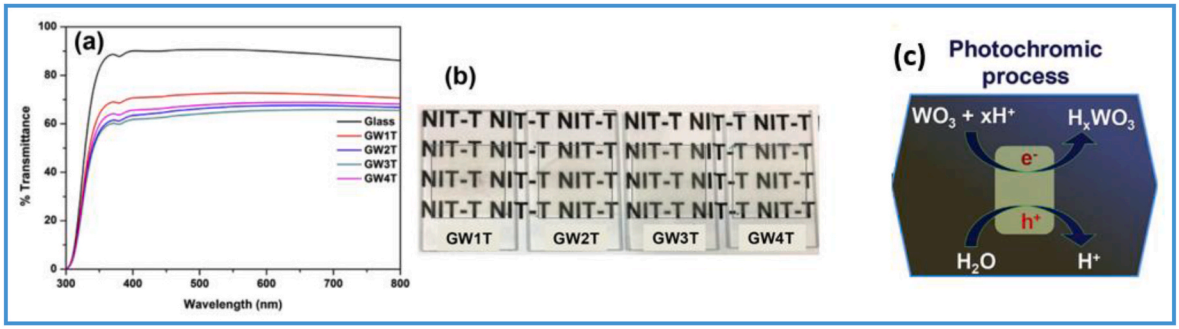

Fig. 23. (a) Transmittance percentage spectra. (b) Photograph of coatings. (c) Photochromic mechanism [101].

mechanism of the photocatalytic degradation of an organic dye on the ZnO/WO_3 composites.

As a continuation of the works on the photochromism between two solid oxides with Schottky barriers, we examined in our group the exceptional photochromism exhibited by a heterojunction composite powder, prepared *via* mechanical mixing into an agate mortar of adequate ZnO and MoO_3 commercial samples (provided by Alfa Aesar: CAS-1314-13-2, D03Y023 and CAS-1313-27-5, E01S050) [105]. The composite materials prepared from the raw mechanical grinding of the two ZnO and molybdenum oxide commercial powders were characterised in terms of the photochromic contrast between the bleached and coloured states, photochromic kinetics for the colouring mode, and reversibility (bleaching mode). The photochromic intensity was revealed to be clearly correlated to the intensity of the UV-light excitation source, demonstrating that the proposed powder mixture can reversibly change its colour in a few minutes under solar irradiation,

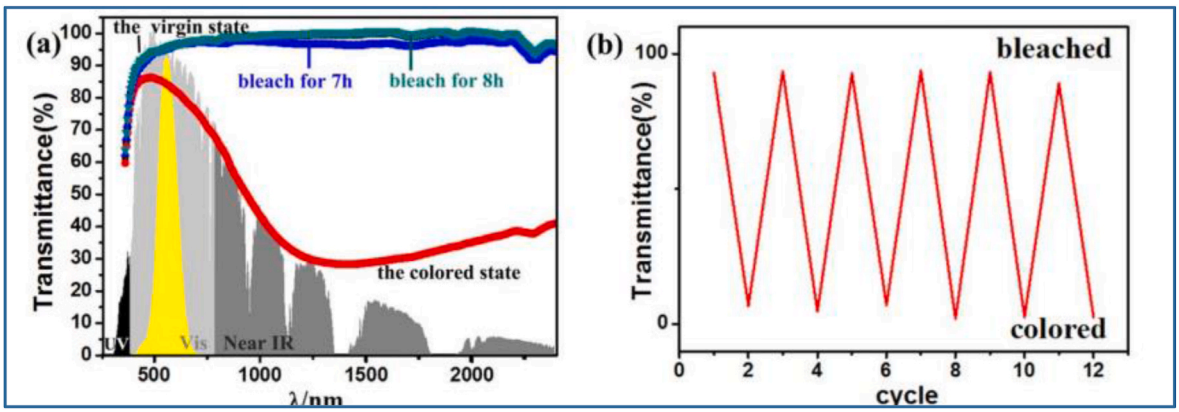

Fig. 24. Photochromic properties of WO_3/WO_3 homojunction composite: (a) transmittance spectra in the solar radiation range (350–2600 nm) before/after irradiation and after being kept in the dark for different times; (b) the transmittance of a water-based suspension of the composite sample at 1000 nm after six cycles [92].

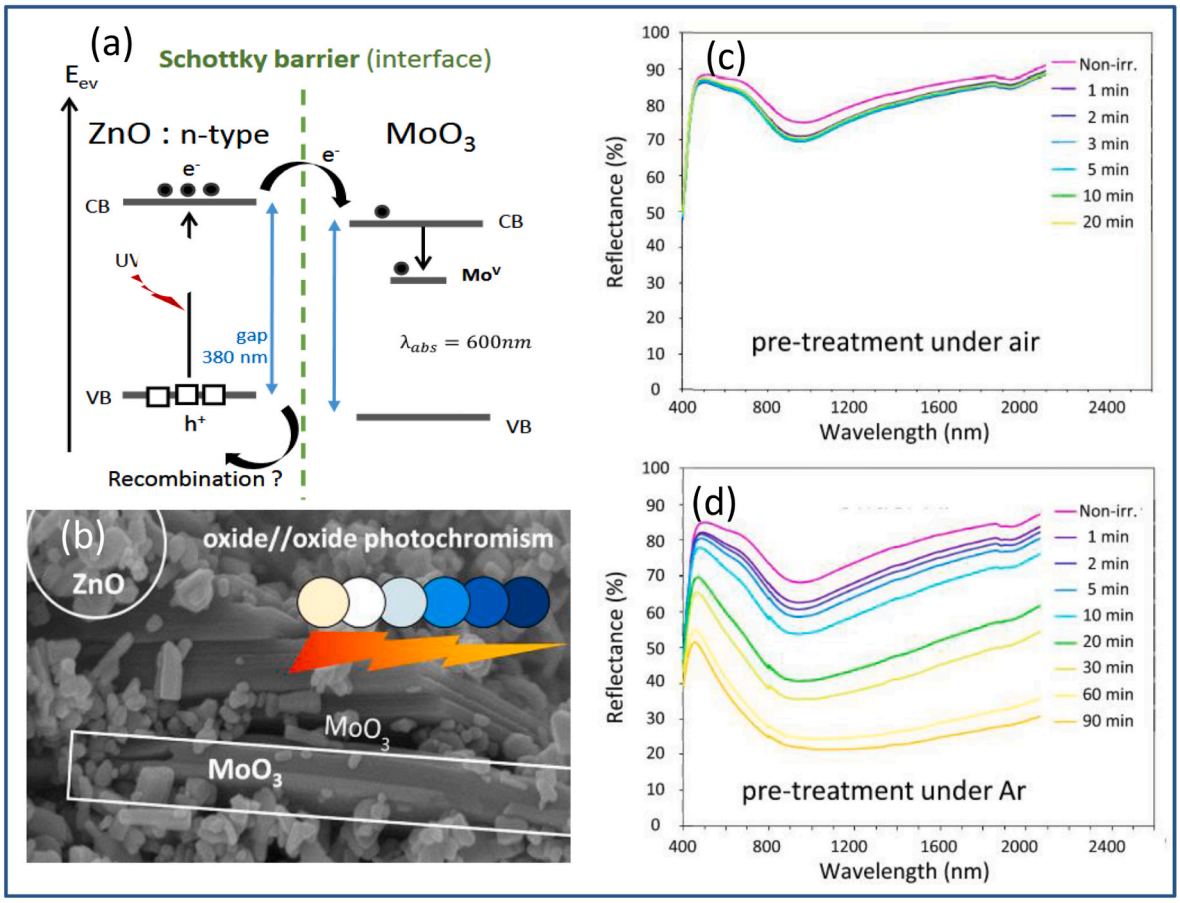

Fig. 25. Electron/hole recombination scheme at the Schottky barrier at the ZnO/MoO_3 interface: (a) SEM image of the as-prepared ZnO/MoO_3 mixture; (b) evolution of the reflectance spectra as a function of UV-light irradiation time after pre-annealing treatment in (c) air and (d) argon. Recomposed figure from the articles [105,107].

while self-bleaching is completed in a few hours under dark conditions. Moreover, the possibility of quenching the photochromic effect or tuning the reversible behaviour *via* oxidative gas treatment, has led to the reinterpretation of the redox mechanism initially proposed by Deb et al. in the 1960s, regarding the non-reversible photochromism of WO_3 or MoO_3 caused by the formation of tungsten or molybdenum bronzes [106]. Indeed, a pre-annealing treatment on the ZnO powder under different atmospheres (*e.g.*, air or argon, Fig. 25c and d) shows that the ZnO surface must be oxygen-deficient to act as an efficient reducer for the MoO_3 compound and thereby allow the Schottky barrier creation. From this key observation, a self-looped redox reaction through the MoO_3/ZnO interfaces, owing to the opposite exchange of electrons from the conduction band of the two oxides and the hole recombination of the valence band from oxygen anion exchange, was proposed. Such material combinations with exceptional colouring efficiency open a new pathway in the industry of inorganic photochromic materials, allowing the development of advanced photochromic smart films in the near future.

After that, our team evidenced that the creation of ZnO oxygen-poor

surfaces is a key element to achieve an efficient Schottky barrier at the ZnO/MoO_3 interface, we focused on the "improvement of the photochromism taking place on ZnO/MoO_3 combined material interfaces". We developed in a more recent article several ways to act on the photochromic efficiency: high intensity of the colouring, high kinetics of colouring, and the possibility of bleaching in rather short times to address the potential reversibility of the properties [107]. In the first stage, commercial and homemade (by using a polyol process) ZnO and MoO_3 oxides with different morphologies and different pre-existing electrons inside their CBs were compared in terms of optical properties. This step involves the modulation of the oxygen anion/cation ratio and/or the introduction of aliovalent doping ions into the ZnO matrix. Photographs of the 3 mol% Al-doped ZnO and MoO_3 oxides prepared from the polyol process are shown in Figure c8. In the second stage of our protocol, the characterisation of the colouring effect under UV irradiation was investigated for different mixtures obtained from various types of ZnO and MoO_3 oxides. The colouring efficiency of the oxide/oxide system was increased owing to the pre-existing electrons in the conductive band of ZnO created by aliovalent doping (with aluminium III species) from a polyol synthesis route. Furthermore, the ZnO NPs obtained from polyol showed the best properties because of their very large surface area, which is further oxygen deficient from the reducing properties of the polyol used for synthesis. The characterisation of the colouring effect under irradiation of the ZnO/MoO_3 mixture prepared from commercial powder and that prepared from the compounds obtained from the polyol process, for confirmation, is depicted in Fig. 26. Finally, it can be noted that it was discovered, that the colouring and bleaching efficiencies show strong interdependence: deeper is the blue colour obtained after irradiation and less reversible is the photochromism. To apply such materials in large-scale applications, it is necessary to overcome the issue of the deterioration of the bleaching efficiency when the photochromic colouring is too pronounced. This will be of great importance for further studies.

3. Contribution of rare earth or transition elements to photochromism

In addition to transition metals, rare earth elements (REs) can actively contribute to the photochromic properties. The optical contrast generated under irradiation can be reinforced by the insertion of an emitting centre. Intriguingly, the introduction of a luminescent element into a photochromic matrix leads to the revealing of the colour switch in emission under excitation at a specific wavelength. These advantageous photoluminescent modulations can provide new platforms in counterfeiting, active sensors, or new generation non-destructive controllers applications, since the reading of the specific properties is conditioned

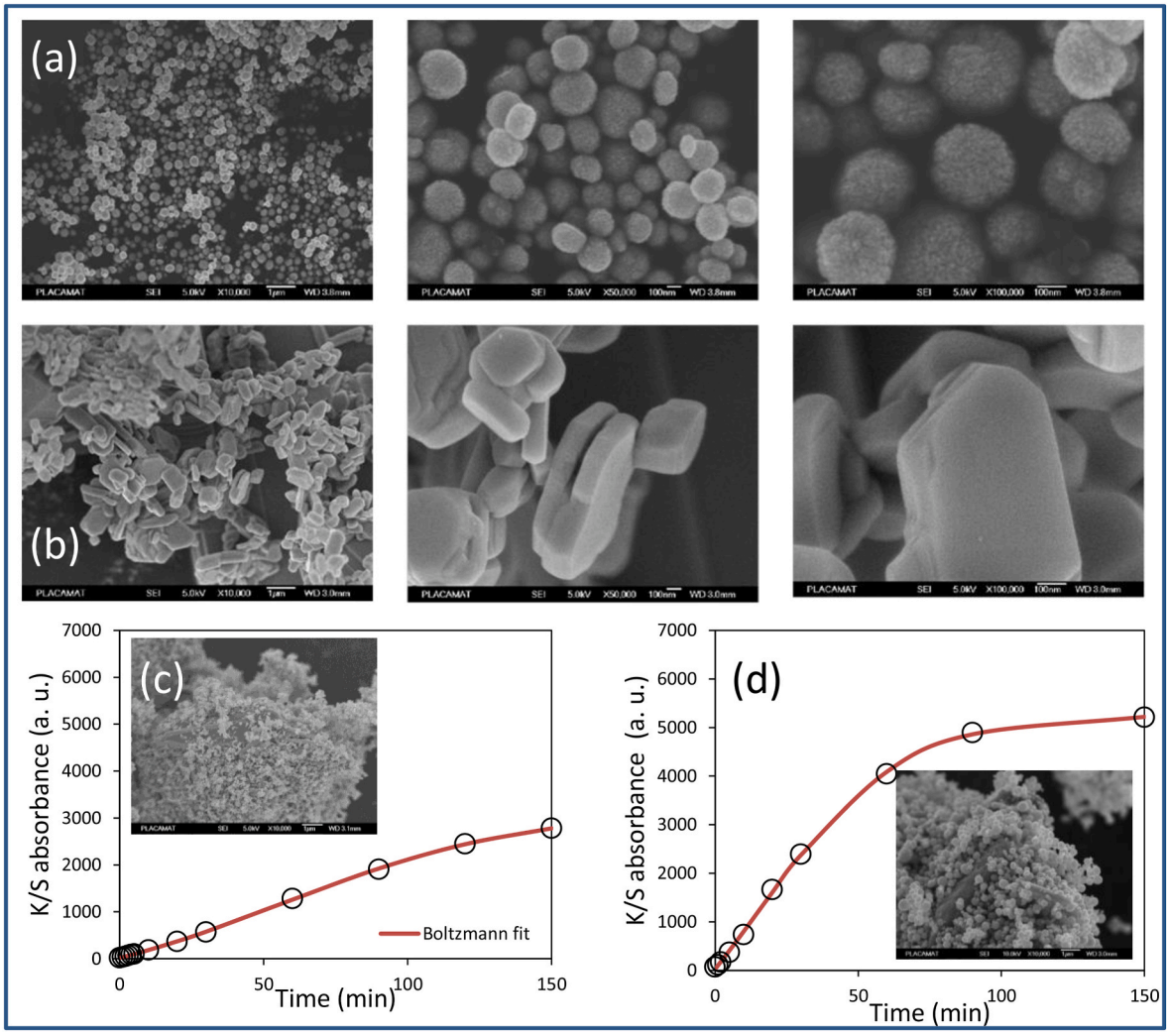

Fig. 26. SEM pictures of the (a) $Zn_{0.97}Al_{0.03}O$ oxide and (b) MoO_3 oxide prepared *via* the polyol process. Comparison of the colouring properties (K/S Kubleka-Munk absorbance coordinates) of a ZnO/MoO_3 composite material issued from commercial ZnO and MoO_3 powder, and the $Zn_{0.97}Al_{0.03}O/MoO_3$composite material prepared from the two oxides obtained from the polyol process. Recomposed figure from the article [107].

by the knowledge of the appropriate irradiation characteristics (safety inks). Different approaches have been developed to realize this, including the modulation of the absorption range in order to induce variation in the intensity of the luminescent centre or its spectral distribution. Furthermore, punctual defects can manifest at the start of photochromism, resulting from redox reactions, leading to the appearance or disappearance of emission bands. Because of their optical and chemical properties, rare earth elements constitute a rich source of inspiration for chemists. This part of our review focuses on examples involving the contribution of rare earth elements.

3.1. Competitive absorption between PC absorption and RE emission

Reabsorption of RE radiative de-excitation by the photochromic centre should result in the potential control of the emission intensity. $REW_2O_6(OH)_6$ (RE = Y^{3+}, Eu^{3+}) is known to undergo intervalence charge transfer transitions (IVCT) originating from photo-activated d-d transitions between neighbouring tungsten cations. The photoreduction of W^{+6} into W^{+5} led to a bluish matrix [108]. Additional UV absorption bands result from the electron charge transfer between W and O and Eu–O. Observation of the red 4f-4f emission of Eu^{3+} ions under direct excitation is conditioned by non-radiative competitive processes, and the darkening of the matrix leads to the progressive quenching of the visible Eu^{3+} emission (Fig. 27). The reversibility of the optical properties was obtained under heat treatment at 180 °C for 15 min.

In $Na_{0.5}Bi_{4.5}Ti_4O_{15}$, Sm^{3+}, Pr^{3+}, or Er^{3+} ions were introduced as doping elements by Zhang et al. [109]. If the emission is tailored by the intensity of the absorption band stabilised under irradiation, the origin of the matrix colouring is linked to the stabilisation of punctual defects such as Na, Bi, and O vacancies during the heat treatment required by the synthesis process. The photochromic properties are ascribed to non-radiative energy transfer by dipole-dipole interactions between the doping element and punctual defects that act as coloured centres. Because of the Sm^{3+}, Pr^{3+}, or Er^{3+} energy diagram specificity (λ_{exc} Sm^{3+} < λ_{exc} Pr^{3+} < λ_{exc} Er^{3+}), the luminescent switching contrast is higher for the lowest energy excitations, and the resulting emission wavelength is observed at higher energies (λ_{em} Sm > λ_{em} Pr > λ_{em} Er) (Fig. 28).

A complementary study showed that a poling treatment applied to this compound can modulate the intensity of photochromism, as demonstrated by Li et al. [110]. This is due to the structural modification of the poled surface into long-range ordered ferroelectric domains. The emitting properties of Er^{3+} were checked under IR excitation in order to study the luminescence response without simultaneous modification of the photochromic centres. The resulting Er^{3+} up-conversion emission in the visible range was significantly reduced in the poled zone. The poling treatment is, by consequence, presented as an efficient tool to tailor the emission modification contrast on a photochromic surface.

In addition, rare earth-doped niobate compounds such as $Na_{0.5}Bi_{2.5}Nb_2O_9$ or ferroelectrics $(K,Na)NbO_3$ are now considered as a new class of solid-state reversible photochromic luminescent materials [111–113]. Similar to the previous titanates, the heat treatments induced the volatilisation of alkali elements, leading to the creation of cationic vacancies within the host lattice. The overlap between the absorption of the resulting colour centres initiated by irradiation and the spectral distribution of the rare-earth doping elements makes the luminescent switching effect possible (Fig. 29). The amplitude of the remaining luminescence can be modulated as a function of the concentration of punctual defects induced by the firing temperature. Reversibility was obtained after heat treatment at 230 °C for 10 min. Aging of the Sm^{3+}-and Ho^{3+} doped photochromic materials has been tested over 10 cycles [113,114].

Successful control of modulation luminescence has also been achieved by Zhang et al. in Sr_2SnO_4:Eu^{3+} stannate [115]. Sr vacancies are stabilised within the host lattice with a concentration that is dependent on the firing temperature according to the following equation:

$$2Eu^{3+} \xrightarrow{3Sr^{2+}} 2Eu^{\bullet}_{Sr} + V''_{Sr}$$

Under ultraviolet excitation (280 nm), the Sr vacancy traps a hole to form a coloured centre. The compound turned from white to purple. Reversibility is obtained with excitation at longer wavelengths in the blue range (450 nm). The introduction of trivalent europium improves

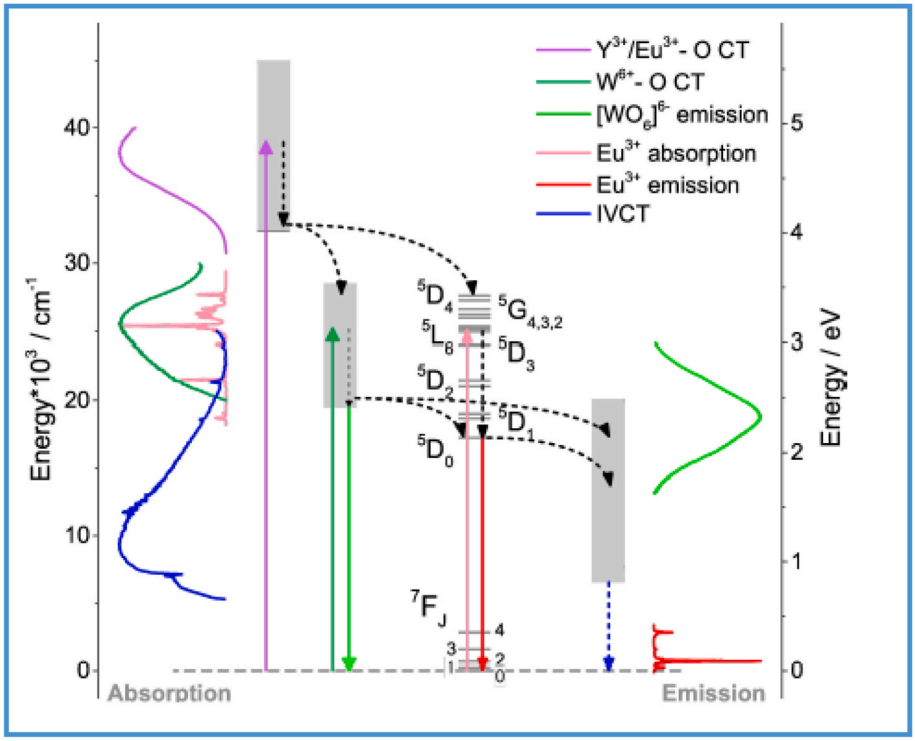

Fig. 27. Energy diagrams illustrating energy transfers into the $TRW_2O_6(OH)_3$ (TR = Y^{3+},Eu^{3+}) compound [108].

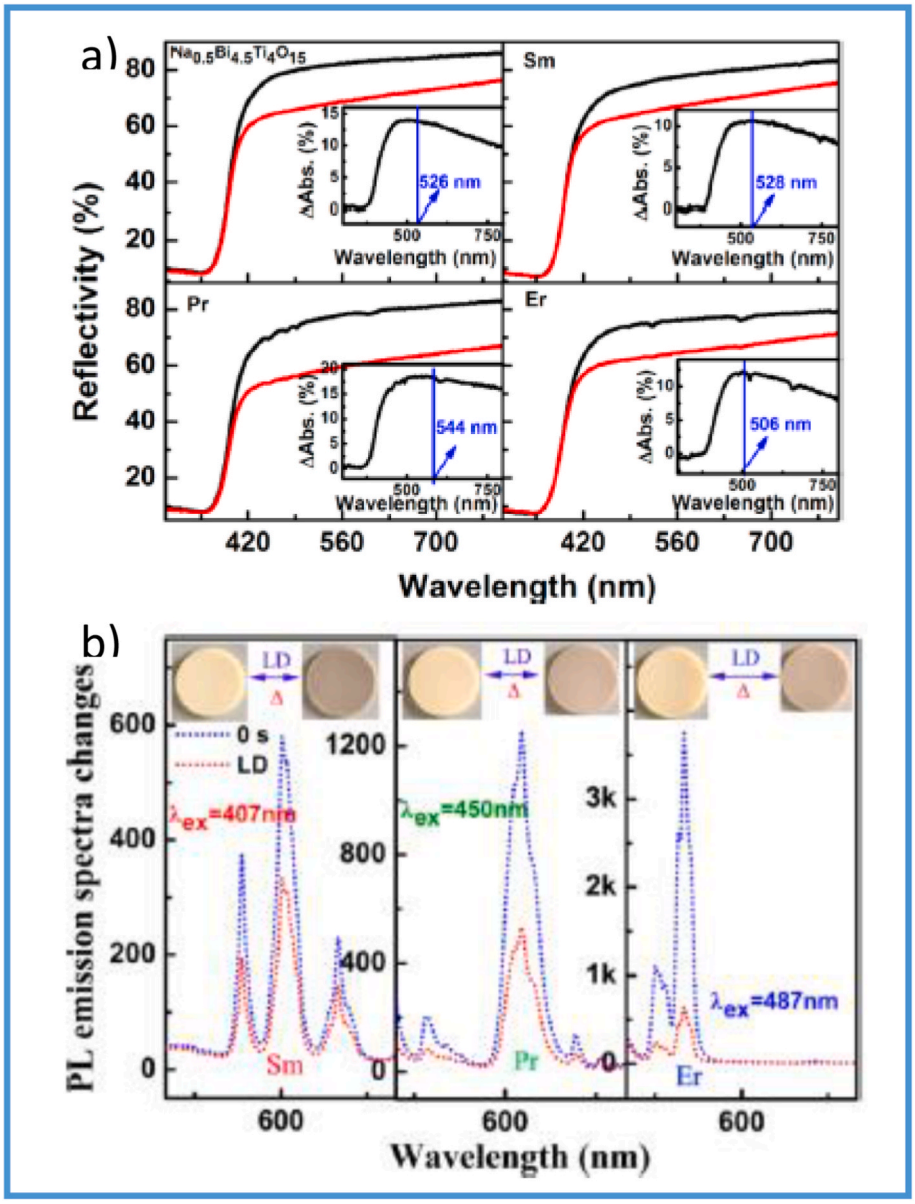

Fig. 28. (a) Diffuse reflectance spectra and (b) emission spectra before and after UV irradiation for 20 s at 407 nm of $Na_{0.5}Bi_{4.5}Ti_4O_{15}$ dopé RE^{3+} (RE = Sm, Pr et Er) shaped as a ceramic [109].

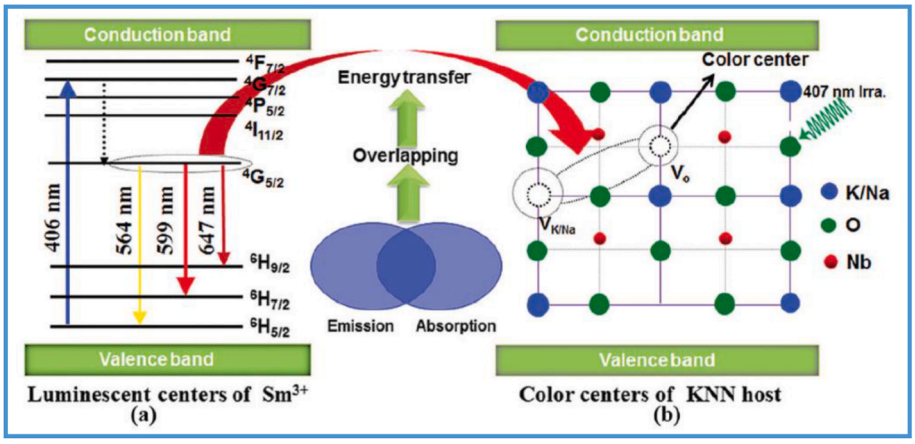

Fig. 29. Schematic diagram of the energy transfer mechanism in the Sm doped KNN host: (a) luminescent centres of Sm^{3+} ions and (b) colour centres of the KNN host [113]. (For interpretation of the references to colour in this figure legend, the reader is referred to the Web version of this article.)

the optical contrast of the bulk materials; however, a significant quenching of the expected Eu^{3+} ions was observed. In this case, the oxidation state of the rare earth clearly contributed to the improvement of the photochromic response. Excellent reversibility of luminescence quenching/recovery was observed over 20 cycles of irradiation. However, Kamimura et al. mentioned in a previous article that they did not detect any Eu^{2+} or Eu^{3+} emission in this matrix, which indicates that the released holes recombine radiatively with the Eu^{2+} ions [116]. Cycling of the white/purple photochromism was observed over 10 cycles. Photoluminescent switching of this compound was also reported when it was doped with Er^{3+} ions [117]. A 980 nm excitation wavelength was chosen to highlight the variation of the up-converted emission at 550 nm, in the green range, as a function of the source power or the grain size (a higher concentration of punctual defects is reported for the smallest grains owing to a higher specific surface area). This green emission is thus strongly affected by the photochromic properties of the stannate. It is weakened under UV irradiation, but a full recovery is observed at 450 nm in parallel with the discolouration of the host lattice. In complement, the modulation of Eu^{2+} emission was reported recently by Lv et al. in the $(Ca,Sr,Ba)_5(PO_4)_3F$ matrix. The authors proposed to tune the photochromic properties through the substitution the alkali earth metal and thus to observe significant changes in the luminescence [118].

3.2. RE and transition metals elements at the origin of the PC centres

Although REs can be directly involved in the photochromism mechanism, their radiative de-excitation can be completely quenched. Different phosphate compounds were investigated. The Eu^{2+}, Gd^{3+} doped $Ba_{10}(PO_4)_6ClF$ presents under 254 nm irradiation, a bulk colour modification from white to amethyst; a total bleaching is observed by J. Guifang et al. under irradiation at 523 nm or a thermal treatment at 200 °C [119]. The colouring is linked to the introduction of the RE element as the non-doped matrix remains white under UV irradiation. After UV irradiation, the Eu^{2+} excited electron is promoted on the $4f^6$ 5 d^1 orbitals and then delocalized through the conduction band before being trapped on the defect centre energy level. The co-doping with a trivalent cation as Gd^{3+} has to be balanced, which increases the concentration of punctual defect sites and thus favours the oxidation of europium up to trivalent oxidation state. After irradiation or heat treatment, the trapped electron is released (potential interaction with phonons or photons is mentioned) and reaches the conduction band. Its transfer to europium and the oxidation of this last one initiates the bleaching of the compound. Similar observations were reported for the $Ca_2Ba_3(PO_4)_3F$ host lattice photochromic properties. The authors highlighted the Eu^{2+} ions concentration in the colouring/bleaching process and its cycling reproducibility. The intensity of the green emission is affected by the concentration of punctual defects at the origin of the photochromic centres [120].

In fluorite matrices such as MF_2 (M = Ca, Sr, Ba), ionising radiation or heating in metal vapours can partly reduce Y^{3+}, Gd^{3+}, La^{3+}, Ce^{3+}, Lu^{3+}, and Tb^{3+} in the divalent oxidation state: intense absorption bands of the divalent RE cations appear [121–123]. Additional defect centres as acceptors F_3^- or F_2 are also listed as taking part in the absorption phenomena. Because of a high crystal field, it has been demonstrated in these halide matrices, that the highest atomic number of the alkaline-earth element, the highest energy bandgap of the host lattice. The third ionisation potential of lanthanides is known to be weak, as they are very stable in the trivalent oxidation state. Nevertheless, the tendency to generate photochromic centres under irradiation and form a coloured matrix mainly originates from the reduction of the rare earth elements leading to absorption bands in the ultraviolet and visible ranges. Concerning the Lu^{3+}- doped Fluorite, a theoretical approach concluded that the excited photochromic energy level is close to that of the RE lowest d orbitals and this last one may overlap the F^- centre wavefunction. The associated luminescence is due to transition from this admixed resulting energy level to the disturbed lower F-type centre level [123]. If the existence of such species is clearly visible in the absorption graphs, the RE^{2+} luminescence is not reported in the cited articles. The re-oxidation temperature of the RE elements depends not only on the nature of the matrix but also on the nature of the RE.

Moreover, in some specific matrices, it is possible to detect a weak contribution from RE emissions. Within the lanthanide series, Eu is a luminescent ion in both divalent and trivalent oxidation states. Introduced in a matrix such as Eu^{3+}, it can be reduced under irradiation and contributes to the enhancement of the photochromic properties. Not only does it modify the trap level depth within the bandgap, but it also contributes to an increase in its density. The residual luminescence of Eu^{2+} is weak, and Eu^{3+} emission is generally not detected. Several investigations have been conducted on Zn_2GeO_4 [124] and $Sr_3REA(PO_4)_3F$ (RE = Y,Gd, A = Li,Na) [125–128]. The photochromic origin is attributed to the trapping and storage of the excited electron on a punctual defect. The stabilisation of colour defects as F-centres resulting from the capture of an electron by an anionic vacancy is favoured by the presence of this rare earth element, giving rise to the colouring of the matrix from white to grey, cyan, or magenta. A photochromic mechanism is illustrated in Fig. 30.

Competitive absorption-emission mechanisms were also reported on Sm^{3+}-doped $BaZrO_3$ and Eu^{3+}-doped $Sr_3Sn_2O_7$ compounds. The authors underlined the role of the RE^{3+} element in the stabilisation of photochromic absorbing centres and the resulting emission quenching of the 4f-4f transitions [129,130]. The cycling of the properties was also controlled over several irradiation/heating exposure. The role of lanthanides can be highlighted by thermoluminescence measurements [125,126]. The trapped electrons are released by the heat treatment, which gives an indication of the energy location of the defect level within the gap of the materials.

Transition metals can also favour the creation of photochromic centres. Concerning the Ni^{2+}-doped yttrium aluminium gallium garnet or the Cr^{3+}-doped $Mg_4Ga_8Ge_2O_2$ compounds, the overlap between the absorbing centres and the emission spectral distribution in the red-IR range is weak compared to the examples listed before [131,132]. Hence for such compounds, a persistent luminescence was detected which gives a new dimension of these functionalised materials. Thermoluminescence investigation coupled with ESR made possible a better understanding of the nature of traps and the electron dynamic in the process.

3.3. Photochromoluminescent materials: an emerging category

Finally, it is possible to tailor the emission colour based on photochromic properties. The coupling between luminescence and the photochromic effect can result in both the modification of the colour bulk and change in the emission spectral distribution. Eu^{2+}-doped $Ba_3MgSi_2O_8$ is a white compound that exhibits blue 5d-4f luminescence under ultraviolet excitation. Meanwhile, this radiative deexcitation decreases in favour of a new band peaking at 600 nm. The resulting powders are orange in colour, while the global emission, addition of a blue and red component, becomes purple (Fig. 31) [133,134].

For such a matrix, the reductive atmosphere required to stabilise Eu^{2+} during the synthetic route induces the creation of positive oxygen vacancies. The absorption centre is assigned to an unpaired electron trapped at this defect point, similar to the F centre in fluorite alkali halides. A structural distortion caused by a neighbouring cation introduced as an impurity can also stabilise other punctual defects on which the electron can be captured. The 450 nm irradiation results in a new absorption band ranging from 430 nm to 600 nm, which involves a decrease in the blue Eu^{2+} emission. The new emission band located at 600 nm is attributed to electron transfer between the two irradiation-induced levels. The mechanism is shown in Fig. 32.

The photochromic process not only generates absorption bands in the visible region but also in the ultraviolet region. In this case, the irradiated compound remains white, but if a redox process of the cation

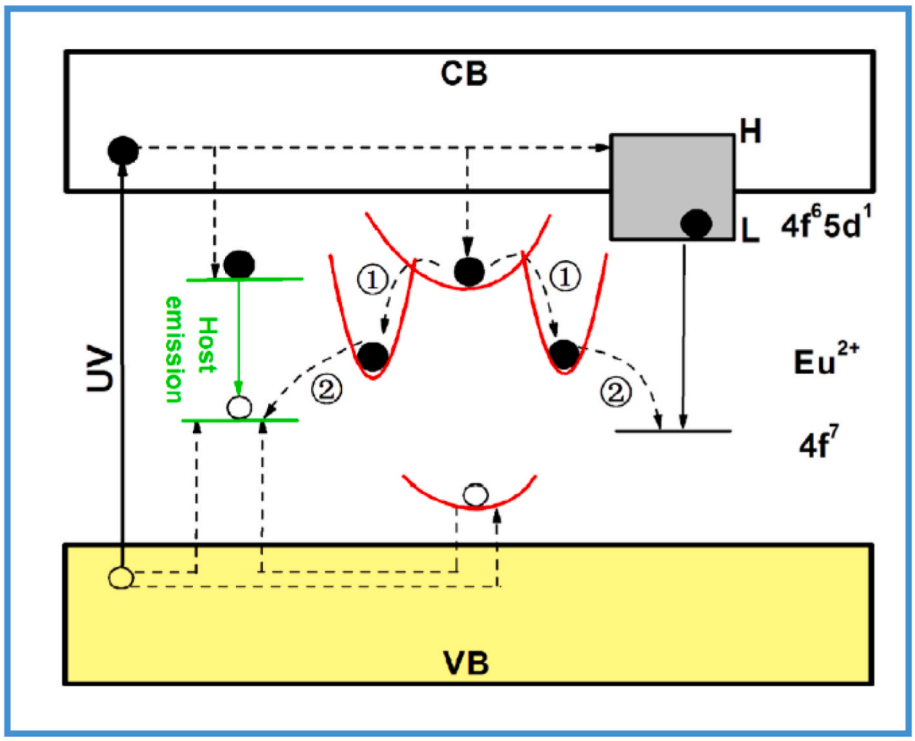

Fig. 30. Schematic illustration of the photochromism mechanism in Zn_2GeO_4 [124].

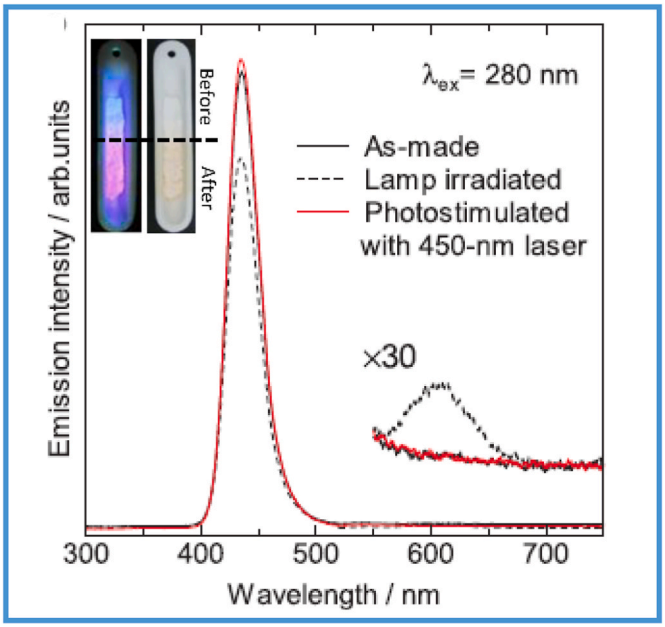

Fig. 31. Emission graphs before and after irradiation at 450 nm. Pictures show the powder colour under 450 nm and under natural light [133,134]. (For interpretation of the references to colour in this figure legend, the reader is referred to the Web version of this article.)

is initiated, a change in the emission spectral distribution is observed. In indium-doped sodium borate glass, short ultraviolet or gamma ray irradiation results in the oxidation of In^+ into In^{2+} or In^{3+} [135]. These metastable species give rise to large emission bands covering the entire visible range. Nonetheless, photo-bleaching was observed during the recording of the emission, indicating the lack of stability of the photochromic-induced species. However, the indium cation redox process can be coupled to the redox mechanism of RE elements such as terbium or cerium, as demonstrated by Chaminade et al. [136–139]. The UV irradiation of Ce^{3+}-doped Rb_2KInF_6 elpasolite induces a redox process according to the following equation:

$$2Ce^{3+} + In^{3+} \underset{255nm}{\overset{315nm}{\rightleftharpoons}} 2Ce^{4+} + In^{+}$$

The progressive disappearance of Ce^{3+} ions excited at 315 nm is associated with a decrease in the blue emission in favour of the reduction of In^+ cations. The appearance of a new absorption band at 255 nm confirms the existence of this monovalent species, in which the radiative $5s^1 5p^1 \rightarrow 5s^2$ transition is detected in the orange range. A nice on-off effect of the cation emission was obtained. However, this excitation at a short UV range leads to the simultaneous re-oxidation of indium and recovery of cerium in the trivalent oxidation state. This reversible phenomenon has been attributed to the crystal structure in which the overlap of the 5d Ce^{3+} orbitals with the s-p orbitals of the In^+ ions and a potential metal-metal hybridisation (Fig. 33). The cycling of this redox process has been checked over five cycles under UV irradiation, but it shows an ageing phenomenon. Recently, attempts have been made to observe a similar redox phenomenon in close structural compounds. K_2NaInF_6 elpasolite and K_3InF_6 cryolite were doped with Ce. Both compounds present comparable blue/orange switches in their optical properties under UV irradiation. A light shift of the Ce^{3+} and In^+ emissions is observed in agreement with the change in the ionocovalent nature of the chemical bonding and the crystal field effect at the cationic site [140].

4. Conclusions

In the first part of this review, the importance of the well-established WO_3 wide bandgap semiconductor, used as the archetypical inorganic oxide for illustration, was illustrated and complemented through its sister oxides, MoO_3, V_2O_5, TiO_2, and Nb_2O_5. Their synthesis *via* new synthetic routes as nanoparticles can effectively optimise the

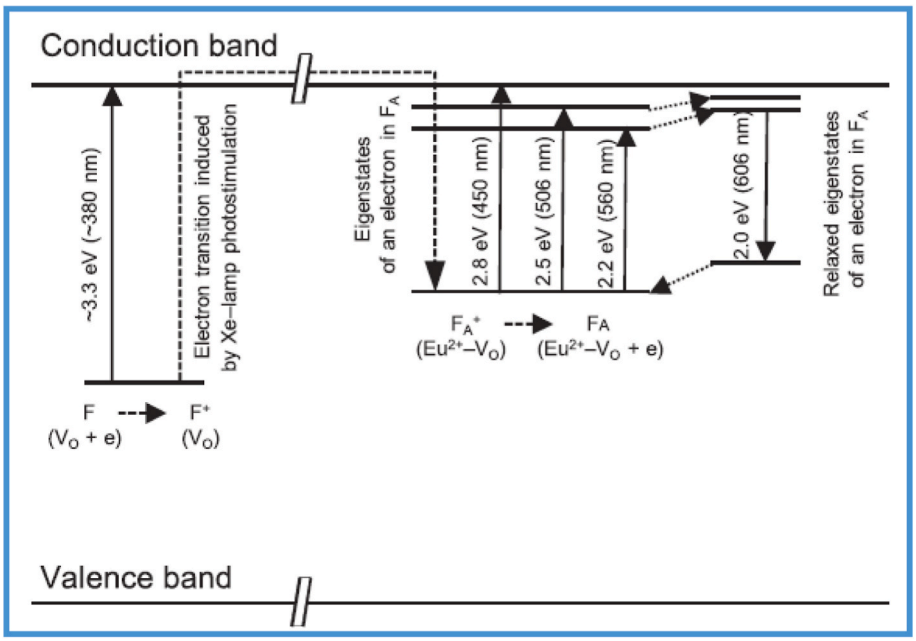

Fig. 32. Illustration of the luminescent photochromic properties of $Ba_3MgSi_2O_8:Eu^{2+}$ [133].

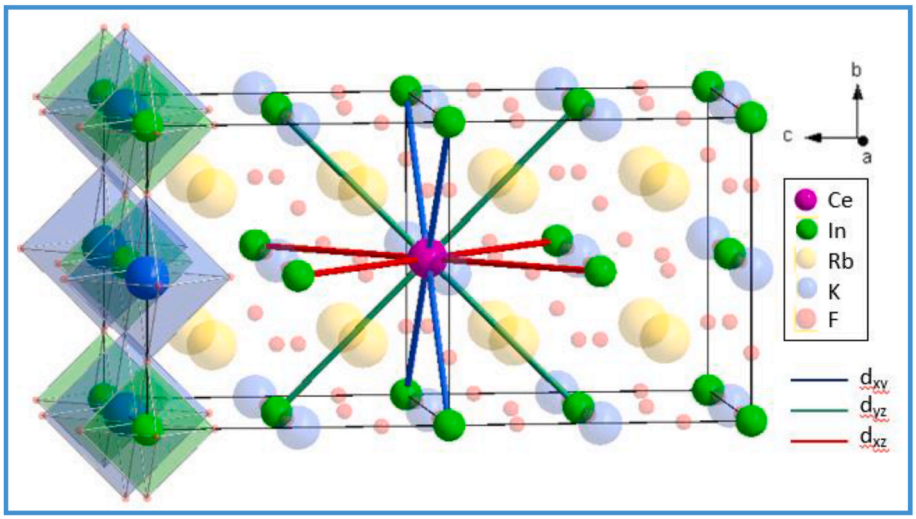

Fig. 33. Illustration of crystal structure of Rb_2KInF_6 unit, highlighting the vicinity of Ce^{3+} and In^{+} cations [140].

photochromic behaviour (*e.g.*, in terms of the optical contrast between photobleached and coloured states, the colouring and bleaching kinetics, the reversibility (full/partial bleaching), the cyclability). Achieving the complete photobleaching of a previously irradiated sample through a reasonable darkening time, however, remains of key importance which is difficult to reach while the mechanism involved a single compound. Recent improvements in this direction were realised by associating two semiconducting oxides bounded by a Schottky barrier at the interface (ZnO–MoO_3 recent developments were deeply discussed), allowing for charge depletion at the start of the photochromic effect (electron/hole separation) to enhance the redox properties.

In the second part, we highlighted the contribution of rare earth elements (RE), such as europium or cerium, in widening the colourimetric contrast in terms of both intensity and spectral distribution, and by extension, in designing next-generation photochromic devices. The RE elements as well as transition metals play a significant role in the stabilisation of photochromic centres. Depending on the processes which are involved, a quenching of the emission or reversely a new luminescence resulting from defects or from these doping elements can be detected. Furthermore, RE elements, as luminescent ions that can be involved in intra-crystal redox reactions, can be used for the manifestation of new photochromoluminescent properties, defined as the capacity to change the material emission spectra from its previous regime (typically in the UV range). The recent discovery of bistable alkaline indium fluorides, with the capacity to achieve huge contrast changes in the emission spectra (*i.e.*, from orange to blue) in a controllable, reverse, and repeatable manner, has opened the window for highly advanced applications, such as state-of-the-art data storage materials.

To conclude, photochromism is the consequence of a large panel of photoinduced-mechanisms, linked to various redox reactions implying electronic transfers from one donor to one acceptor, the major part of which being reversible through further irradiation or thermal treatment. The versatility of the inorganic materials offers a coloured panel ranging from the visible to near-infrared wavelengths. Coupled with the properties of luminescence, photochromism makes it possible to obtain highly multifunctionalized materials that should better meet society's

requirements in terms of detection/sensing materials.

CRediT authorship contribution statement

Y. Badour: Formal analysis, Writing – original draft, Writing – review &amp editing. **V. Jubera:** Investigation, Supervision, Methodology, review & editing, Writing – original draft, Visualization, Project administration, Validation. **I. Andron:** Formal analysis. **C. Frayret:** Validation, Visualization, Formal analysis. **M. Gaudon:** original draft, Writing – review &amp editing, Funding acquisition, Investigation, Methodology, Validation.

Declaration of competing interest

The authors declare that they have no known competing financial interests or personal relationships that could have appeared to influence the work reported in this paper.

Acknowledgements

The authors thank the CNRS, the Region Nouvelle d'Aquitaine. The PhD grant of Y. Badour and I. Andron were supported by the University of Bordeaux in the frame of funding attributed by the French ministry of research and the French National Research Agency, ANR 2016 program (ANR-16-CE08-0029), respectively.

References

[1] W. Marckwald, Ueber phototropie, Z. Phys. Chem. 30U (1) (1899) 140–145, https://doi.org/10.1515/zpch-1899-3007. De Gruyter Oldenbourg | Published online: January 22, 2017.
[2] E.Y. Fischer, Y. Hirshberg—in memoriam, J. Chem. Educ. 40 (3) (1963) 112–113, https://doi.org/10.1021/ed040p112.
[3] Y. Hirshberg, Reversible formation and eradication of colors by irradiation at low temperatures. A photochemical memory model, J. Am. Chem. Soc. 78 (10) (1956) 2304–2312, https://doi.org/10.1021/ja01591a075.
[4] R. Macnair N, Photochromism and phototropism : a terminology poll, Photochem. Photobiol. 14 (1971) 759–761, https://doi.org/10.1111/j.1751-1097.1971.tb06216.x.
[5] K. Nakatani, J. Piard, P. Yu, , et al.R. Métivier, Introduction: organic photochromic molecules, in: He Tian, Junji Zhang (Eds.), Photochromic Materials: Preparation, Properties and Applications, first ed., Wiley-VCH Verlag GmbH & Co. KGaA, 2016. ©Published 2016 by Wiley-VCH Verlag GmbH & Co. KGaA.
[6] I.A. Rostovtseva, N.A. Voloshin, E.V. Soloveva, A.V. Chernyshev, I.A. Metelitsa, , et al.A.V. Metelitsa, « Spiropyrans and spirooxazines » 67 (8) (2018) 1476–1481, https://doi.org/10.1007/s11172-018-2242-0.
[7] R.D. Kirk, The luminescence and tenebrescence of natural and synthetic sodalite, Am. Mineral. 40 (1&2) (1955) 22–31.
[8] D. Kondo, D. Beaton, Hackmanite/Sodalite from Myanmar and Afghanistan, Gems Gemol. 45 (1) (2009) 38–43, https://doi.org/10.5741/GEMS.45.1.38.
[9] V.A. Barachevsky, Negative photochromism in organic systems, Rev. J. Chem. 7 (3) (2017) 334–371, https://doi.org/10.1134/S2079978017030013.
[10] T. Yamaguchi, A. Maity, V. Polshettiwar, M. Ogawa, Negative photochromism based on molecular diffusion between hydrophilic and hydrophobic particles in the solid state, Inorg. Chem. 57 (7) (2018) 3671–3674, https://doi.org/10.1021/acs.inorgchem.7b03132.
[11] C. Bohne, , et al.R.H. Mitchell, Characterization of the photochromism of dihydropyrenes with photophysical techniques, J. Photochem. Photobiol. C Photochem. Rev. 12 (2) (2011) 126–137, https://doi.org/10.1016/j.jphotochemrev.2011.08.001.
[12] D. Fanghanl, C. Timpe, V. Orthman, Photochromic compounds with N=N and C=N chromophores, in: Organic Photochromes, Springer, Boston, MA, 1990, pp. 105–175, https://doi.org/10.1007/978-1-4615-8585-5_3.
[13] M. Irie, T. Fukaminato, K. Matsuda, , et al.S. Kobatake, Photochromism of diarylethene molecules and crystals: memories, switches, and actuators, Chem. Rev. 114 (24) (2014), https://doi.org/10.1021/cr500249p, 12174-12277.
[14] R. Tällberg, B.P. Jelle, R. Loonen, T. Gao, , et al.M. Hamdy, Comparison of the energy saving potential of adaptive and controllable smart windows: a state-of-the-art review and simulation studies of thermochromic, photochromic and electrochromic technologies, Sol. Energy Mater. Sol. Cells 200 (2019) 109828–109858, https://doi.org/10.1016/j.solmat.2019.02.041.
[15] H.J. Hoffmann, The use of silver salts for photochromic glasses, Stud. Org. Chem. 40 (1990) 822–854, https://doi.org/10.1016/B978-044451322-9/50026-9.
[16] G. Gomez, Abécédaire de Chimie Organique, 2019. https://tice.ac-montpellier.fr/ABCDORGA/ORGANIQU.htm.
[17] B.V. Gemert, The commercialization of plastic photochromic lenses: a tribute to john crano, Mol. Cryst. Liq. Cryst. 344 (1) (2000) 57–62.
[18] R. Winder, Photochromes. Sunlight Express, Chemistry & Industry, London (UK), 2006, pp. 20–21.
[19] J. Jiyue, D. Yongqiu, and Y. Zhiyong, « Photochromic Water-Based Nail Polish and Preparation Method Thereof », CN 110200835.
[20] O.J.X. Morel, R.M. Christie, Current trends in the chemistry of permanent hair dyeing, Chem. Rev. 111 (4) (2011) 2537–2561, https://doi.org/10.1021/cr1000145.
[21] H. Rosset, Security Element Having a Variable Optical Effect and Security Sheet or Document or Article Comprising it, 2010. FR 2933428.
[22] M. Akiyama, Blue-green light photochromism in europium doped $BaMgSiO_4$, Appl. Phys. Lett. 97 (18) (2010) 181905–181909, https://doi.org/10.1063/1.3509417.
[23] M. Lescinsky, Holographic recording onto photochromic spiropyran and its application to holographic interferometry, Ceskoslovensky Cas. Fyziku 5 (2) (1972) 104–105.
[24] N. Crespo-Monteiro, N. Destouches, L. Nadar, S. Reynaud, F. Vocanson, J. Y. Michalon, Irradiance influence on the multicolor photochromism of mesoporous TiO_2 films loaded with silver nanoparticles, Appl. Phys. Lett. 99 (17) (2011) 173106–173110, https://doi.org/10.1063/1.3653282.
[25] N.I. Fernandes, G. Poirier, M. Nalin, Thermo and photochromic properties of Na_2O–WO_3–$SbPO_4$ glasses, Solid State Ionics 181 (23–24) (2010) 1125–1130, https://doi.org/10.1016/j.ssi.2010.06.011.
[26] G.P. Smith, Photochromic glasses: properties and applications, J. Mater. Sci. 2 (2) (1967) 139–152.
[27] R. Zhang, The Syntheses, NMR and Photochromic Properties of Modified Dimehtyldihydropyrenes, Thesis Department of Chemistry, University of Victoria, 2007, ISBN 978-0-494-41217-6.
[28] H. Bouas-laurent, H. Dürr, Organic photochromism, J. Photochem. Photobiol., B 73 (4) (2001) 639–665, https://doi.org/10.1016/1011-1344(88)85081-4.
[29] T. He, J. Yao, Photochromism of molybdenum oxide, J. Photochem. Photobiol. C Photochem. Rev. 4 (2) (2003) 125–143, https://doi.org/10.1016/S1389-5567(03)00025-X.
[30] A. Agranat, Y. Yacoby, A correlation between a dielectric induced photorefractive effect and the photochromic effect, Solid State Commun. 52 (5) (1984) 531–534, https://doi.org/10.1016/0038-1098(84)90870-6.
[31] F. Corà, M.G. Stachiotti, C.R.A. Catlow, C.O. Rodriguez, Transition metal oxide chemistry: electronic structure study of WO_3, ReO_3, and $NaWO_3$, J. Phys. Chem. 101 (1997) 3945–3952, https://doi.org/10.1021/jp963724z.
[32] H. Zheng, J.Z. Ou, M.S. Strano, R.B. Kaner, A. Mitchell, K.K. Zadeh, Nanostructured tungsten oxide - properties, synthesis, and applications, Adv. Funct. Mater. 21 (2011) 2175–2196, https://doi.org/10.1002/adfm.201002477.
[33] P.M. Woodward, A.W. Sleight, T. Vogt, Ferroelectric tungsten trioxide, J. Solid State Chem. 29 (1997) 429–434, https://doi.org/10.1006/jssc.1997.7268.
[34] G.A. de Wijs, P.K. de Boer, R.A. de Groot, G. Kresse, Anomalous behavior of the semiconducting gap in WO_3 from first-principles calculations, Condens. Mater. Phys. 59 (1999) 2684–2689, https://doi.org/10.1103/PhysRevB.59.2684.
[35] B.O. Loopstra, H.M. Rietveld, Further refinement of the structure of WO_3, Acta. Crystallogr. Cryst. Chem. 25 (1969) 1420–1421, https://doi.org/10.1107/S0567740869004146.
[36] E. Salje, The orthorhombic phase of WO_3, Acta .Crystallogr. Cryst. Chem. 33 (1977) 574–577, https://doi.org/10.1107/S0567740877004130.
[37] W.L. Kehl, R.G. Hay, D. Wahl, The structure of tetragonal tungsten trioxide, J. Appl. Phys. 23 (1952) 212, https://doi.org/10.1063/1.1702176.
[38] P. Roussel, P. Labbé, D. Groult, Symmetry and twins in the monophosphate tungsten bronze series $(PO_2)_4(WO_3)_{2m}$ ($2 \leq m \leq 14$), Acta Crystallogr. Sect. B Struct. 56 (2000) 377–391, https://doi.org/10.1107/S0108768199016195.
[39] E. Gebert, R.J. Ackermann, Sub stoichiometry of tungsten trioxide; the crystal systems of $WO_{3.00}$, $WO_{2.98}$, and $WO_{2.96}$, Inorg. Chem. 5 (1966) 136–142, https://doi.org/10.1021/ic50035a033.
[40] A. Hjelm, C. Granqvist, J.M. Wills, Electronic structure and optical properties of WO_3, $LiWO_3$, $NaWO_3$, and HWO_3, Phys. Rev. 5 (1996) 2436–2445, https://doi.org/10.1103/PhysRevB.54.2436.
[41] F. Wang, C.D. Valentin, G. Pacchioni, Electronic and structural properties of WO_3: a systematic hybrid dft study, J. Phys. Chem. 115 (2011) 8345–8353, https://doi.org/10.1021/jp201057m.
[42] S.K. Deb, Opportunities and challenges in science and technology of WO_3 for electrochromic and related applications, Solar Eng. Mat. 92 (2009) 245, https://doi.org/10.1016/j.solmat.2007.01.026.
[43] C. Bechinger, E. Wirth, P. Leiderer, Photochromic coloration of WO_3 with visible light, Appl. Phys. Lett. 68 (1996) 2834, https://doi.org/10.1063/1.116340.
[44] S.K. Deb, Optical and photoelectric properties and color centres in thin films of tungsten oxide, Phil. Mag. 27 (1973) 801–822, https://doi.org/10.1080/14786437308227562.
[45] P. Leiderer, C. Bechinger, E. Wirth, Photochromic coloration of WO_3 with visible light appl, Phys. Lett. 68 (1996) 2834.
[46] C. Bechinger, M.S. Burdis, J.G. Zhang, Comparison between electrochromic and photochromic coloration efficiency of tungsten oxide thin films, Solid State Commun. 101 (1997) 753–756, https://doi.org/10.1016/S0038-1098(96)00703-X.
[47] M. Sun, N. Xu, Y. Cao, J.N. Yao, E.G. Wang, Nanocrystalline tungsten oxide thin film: preparation, microstructure, and photochromic behavior, J. Mater. Res. 15 (2000) 927–933, https://doi.org/10.1557/JMR.2000.0132.
[48] N. Li, Y. Zhao, Y. Wang, Y. Lu, Y. Song, Z. Huang, Y. Li, J. Zhao, Aqueous synthesis and visible-light photochromism of metastable h-WO_3 hierarchical

nanostructures, Eur. J. Inorg. Chem. (2015) 2804–2812, https://doi.org/10.1002/ejic.201500132.
[49] C.S. Blackman, I.P. Parkin, Atmospheric pressure chemical vapor deposition of crystalline monoclinic WO_3 and WO_{3-x} thin films from reaction of WCl_6 with O containing solvents and their photochromic and electrochromic properties, Chem. Mater. 17 (2005) 1583–1590, https://doi.org/10.1021/cm0403816.
[50] X. Dong, Z. Wu, Y. Guo, Y. Tong, X. Liu, L. Zhang, Y. Lu, Rational modification in the photochromic and self-bleaching performance of hierarchical microsphere Cu@h-WO_3/WO_3·nH_2O composites, Solar Eng. Mat. Sol. Cells. 219 (2021) 11078, https://doi.org/10.1016/j.solmat.2020.110784.
[51] H. Miyazaki, M. Inada, H. Suzuki, T. Ota, Molybdenum doping effects on photochromic properties of WO_3 based composite films, J.Cer.Soc.Jap. 121 (2013) 106–108, https://doi.org/10.2109/jcersj2.121.106.
[52] C.O. Avellaneda, L.O.S. Bulhões, Photochromic properties of WO_3 and $WO_{3:X}$ (X=Ti, Nb, Ta and Zr) thin films, Solid State Ionics 165 (2003) 117–121.
[53] Y. Shen, P. Yan, Y. Yang, F. Hu, Y. Xiao, L. Pan, Z. Li, Hydrothermal synthesis and studies on photochromic properties of Al doped WO_3 powder, J. Alloys Compd. 629 (2015) 27–31, https://doi.org/10.1016/j.jallcom.2014.11.218.
[54] S. Mohammadi, M. Sohrabi, A.N. Golikand, A. Fakhri, Preparation and characterization of zinc and copper co-doped WO_3 nanoparticles: application in photocatalysis and photobiology, J. Photo. Photobio. 161 (2016) 217–221, https://doi.org/10.1016/j.jphotobiol.2016.05.020.
[55] S. Balendhran, S. Walia, H. Nili, et al., Two-dimensional molybdenum trioxide and dichalcogenides, Adv. Funct. Mater. 23 (2013) 3952–3970, https://doi.org/10.1002/adfm.201300125.
[56] M.M.Y.A. Alsaif, K. Latham, M.R. Field, Tunable plasmon resonances in two-dimensional molybdenum oxide nanoflakes, Adv. Mater. 26 (2014) 3931–3937, https://doi.org/10.1002/adma.201306097.
[57] M. Rouhani, Y.L. Foo, J. Hobley, Photochromism of amorphous molybdenum oxide films with different initial Mo^{5+} relative concentrations, Appl. Surf. Sci. 273 (2013) 150–158, https://doi.org/10.1016/j.apsusc.2013.01.218.
[58] J.N. Yao, Y.A. Yang, B.H. Loo, Microstructures of electrochromic MoO_3 thin films colored by injection of different cations, J. Phys. Chem. 102 (1998) 1856–1860, https://doi.org/10.1021/jp9825922.
[59] M. Wang, K.J. Koski, Reversible chemochromic MoO_3 nanoribbons through zerovalent metal intercalation, ACS Nano 9 (2015) 3226–3233, https://doi.org/10.1021/acsnano.5b00336.
[60] Y. Song, J. Zhao, Y. Zhao, Supramolecular organic frameworks of cucurbit[n]uril-based [2]pseudorotaxanes in the crystalline state, CrystEngComm 18 (2016) 6502–6512, https://doi.org/10.1039/C6CE01320A.
[61] K. Srinivasa Rao, K.V. Madhuri, S. Uthanna, O.M. Hussain, C. Julien, Photochromic properties of double layer CdS/MoO_3 nano-structured films, Math. Sci. Eng. 2 (2003) 79–86, https://doi.org/10.1016/S0921-5107(03)00078-3.
[62] S. Tomás, M. Arvizu, O.Z. Angel, Effect of ZnSe doping on the photochromic and thermochromic properties of MoO_3 thin films, Thin.Sol. Films 518 (2009) 1332–1336, https://doi.org/10.1016/j.tsf.2009.05.054.
[63] J.P. Pereira-Ramos, R. Messina, J. Perichon, Electrochemical formation of a magnesium vanadium bronze $Mg_xV_2O_5$ in sulfone-based electrolytes at 150°C? J. Appl. Electrochem. 16 (1986) 379, https://doi.org/10.1016/0022-0728(87)87019-5.
[64] H.K. Park, W.H. Smyrl, M.D. Ward, $V2_{O5}X_{er}$ogel films asIntercalation hosts for lithium :I.insertion stoichiometry ,site concentration ,and specific energy, J. Electrochem. Soc. 142 (1995) 15, https://doi.org/10.1149/1.2044133.
[65] S. Nishio, M. Kakihana, Evidence for visible light photochromism of V_2O_5, Chem. Mater. 14 (2002) 3730–3733, https://doi.org/10.1021/cm0204270.
[66] T. Kawahara, Y. Konishi, H. Tada, N. Tohge, J. Nishii, S. Ito, A patterned TiO_2(anatase)/TiO_2(rutile) bilayer-type photocatalyst: effect of the anatase/rutile junction on the photocatalytic activity, Angew. Chem. 114 (2002) 2935, https://doi.org/10.1002/1521-3773(20020802)41:15<2811::AID-ANIE2811>3.0.CO;2-%23.
[67] D. Dambournet, I. Belharouak, K. Amine, Tailored preparation methods of TiO_2 anatase, rutile, brookite: mechanism of formation and electrochemical properties, Chem. Mater. 22 (2010) 1173–1179, https://doi.org/10.1021/cm902613h.
[68] J.G. Li, T. Ishigaki, Brookite → rutile phase transformation of TiO_2 studied with monodispersed particles, Acta Mater. 17 (2004) 5143–5150.
[69] L.S. Daniel, H. Nagai, N. Yoshida, M. Sato, Photocatalytic activity of vis-responsive Ag nanoparticles/TiO_2 composite thin films fabricated by molecular precursor method (MPM), Catalysts 3 (2013) 625–645, https://doi.org/10.3390/catal3030625.
[70] K. Naoi, Y. Ohko, T. Tatsuma, TiO_2 films loaded with silver nanoparticles: control of photochromic, J. Am. Chem. Soc. 126 (2004) 3664–3668, https://doi.org/10.1021/ja039474z.
[71] M. Valden, E. Nommiste, Reversible photodoping of TiO_2 nanoparticles for photochromic application, Chem. Mater. 30 (2018), https://doi.org/10.1021/acs.chemmater.8b04813, 9868-8974.
[72] S.K. Deb, Philos. Mag. 27 (1973) 801–822, https://doi.org/10.1080/14786437308227562.
[73] S. Wang, W. Fan, Z. Liu, A. Yu, X. Jiang, Advances on tungsten oxide based photochromic materials: strategies to improve their photochromic properties, J. Phys. Chem. C 2 (2018) 191–212, https://doi.org/10.1039/c7tc04189f.
[74] T. He, J.N. Yao, Photochromic materials based on tungsten oxide, J. Mater. Chem. 17 (2007) 4547–4557, https://doi.org/10.1039/b709380b.
[75] T. He, Y. Ma, Y.A. Cao, P. Jiang, X. Zhang, W.S. Yang, J.N. Yao, Enhancement effect of gold nanoparticles on the UV-light photochromism of molybdenum trioxide thin films, Langmuir 17 (2001) 8024–8027, https://doi.org/10.1021/la010671q.
[76] J.N. Yao, Y.A. Yang, B.H. Loo, Enhancement of photochromism and electrochromism in MoO_3/Au and MoO_3/Pt thin films, J. Phys. Chem. B 102 (1998) 1856–1860, https://doi.org/10.1021/jp972217u.
[77] J.N. Yao, B.H. Loo, Improved visible-light photochromism in Au/MoO_3 SnO_2, Solid State Commun. 105 (1998) 479–480, https://doi.org/10.1016/S0038-1098(97)10093-X.
[78] T. He, Y. Ma, Y.-A. Cao, W.-S. Yang, J.-S. Yao, Improved photochromism of WO_3 thin films by addition of Au nanoparticles, Phys. Chem. Chem. Phys. 4 (2002) 1637–1639, https://doi.org/10.1039/b108531j.
[79] M.A. Fox, M.T. Dulay, Heterogeneous Photocatalysis. Chem. Rev. 93 (1993) 341–357, https://doi.org/10.1021/cr00017a016.
[80] A.L. Linsebigler, G. Lu, J.T. Yates, Photocatalysis on TiO_2 surfaces: principles, mechanisms, and selected results, Chem. Rev. 95 (1995) 735–758, https://doi.org/10.1021/cr00035a013.
[81] M.A. Quevedo-Lopez, R.F. Reidy, R.A. Orozco-Teran, O. Mendoza-Gonzalez, R. Ramirez-Bon, Enhancement of the photochromic and thermochromic properties of molybdenum oxide thin films by a cadmium sulfide underlayer, J. Mater. Sci. Mater. Electron. 11 (2000) 151–155, https://doi.org/10.1023/A:1008933632515.
[82] Z.G. Zhao, Z.F. Liu, M. Miyauchi, Tailored remote photochromic coloration of in situ synthesized CdS quantum dot loaded WO_3 films, Adv. Funct. Mater. 20 (2010) 4162–4167, https://doi.org/10.1002/adfm.201001198.
[83] B.W. Faughnan, R.S. Crandall, Optical properties of mixed-oxide WO_3/MoO_3 electrochromic films, Appl. Phys. Lett. 31 (1977) 834–836, https://doi.org/10.1063/1.89566.
[84] J.N. Yao, B.H. Loo, K. Hashimoto, F. Fujishima, Photochromic characteristics of mixed WO_3–MoO_3 thin films in alcohol vapors, Ber. Bunsen Ges. Phys. Chem. 95 (1991) 554–556, https://doi.org/10.1002/bbpc.19910950502.
[85] H.M.F. Ahmed, N.S. Begum, Synthesis and characterization of MoO_3–WO_3 composite thin films by liquid phase deposition technique: investigation of its photochromic properties, Bull. Mater. Sci. 36 (2013) 45–49, https://doi.org/10.1007/s12034-013-0422-y.
[86] Y. Liu, H.Z. He, J. Li, W.Z. Li, Y.H. Yang, Y.M. Li, Q.Y. Chen, ZnO nanoparticle-functionalized WO_3 plates with enhanced photoelectrochemical properties, RSC Adv. 5 (2015) 46928–46934, https://doi.org/10.1039/C5RA03918E.
[87] T. He, Y. Ma, Y.A. Cao, H.M. Liu, W.S. Yang, J.N. Yao, Comparison between the effects of TiO_2 synthesized by photoassisted and conventional sol–gel methods on the photochromism of WO_3 colloids, J. Colloid Interface Sci. 279 (2004) 117–123, https://doi.org/10.1016/j.jcis.2004.06.053.
[88] Y.Y. Song, Z.D. Gao, J.H. Wang, X.H. Xia, R. Lynch, Multistage coloring electrochromic device based on TiO_2 nanotube Arrays modified with WO_3 nanoparticles, Adv. Funct. Mater. 21 (2011) 1941–1946, https://doi.org/10.1002/adfm.201002258.
[89] R.G. Palgrave, I.P. Parkin, Aerosol assisted chemical vapour deposition of photochromic tungsten oxide and doped tungsten oxide thin films, J. Mater. Chem. 14 (2004) 2864–2867, https://doi.org/10.1039/b406337f.
[90] H. Yang, X. Li, A. Wang, Y. Wang, Y. Chen, Photocatalytic degradation of methylene blue by MoO_3 modified TiO_2 under visible light, Chin. J. Catal. 35 (2014) 140–147, https://doi.org/10.1016/S1872-2067(12)60731-1.
[91] S.H. Elder, F.M. Cot, Y. Su, S.M. Heald, A.M. Tyryshkin, M.K. Bowman, Y. Gao, A. G. Joly, M.L. Balmer, A.C. Kolwaite, K.A. Magrini, D.M. Blake, The discovery and study of nanocrystalline TiO_2-(MoO_3) core–shell materials, J. Am. Chem. Soc. 122 (2000) 5138–5146, https://doi.org/10.1021/ja992768t.
[92] N. Li, T. Cao, T. Chang, S. Long, P. Jin, Selective photochromism in a self-coated WO_3/WO_{3-x} homojunction: enhanced solar modulation efficiency, high luminous transmittance and fast self-bleaching rate, Nanotechnology 30 (2019) 255703, https://doi.org/10.1088/1361-6528/ab0778.
[93] Y. Liu, H. He, J. Li, W. Li, Y. Yang, Y. Li, Q. Chen, ZnO nanoparticle-functionalized WO_3 plates with enhanced photoelectrochemical properties, RSC Adv. 5 (2015) 46928–46934.
[94] O. Oderinde, M. Kang, M. Kalulu, F. Yao, G. Fu, Facile synthesis and study of the photochromic properties of deep eutectic solvent-templated cuboctahedral-WO_3/MoO_3 nanocomposites, Superlattice, Micro 125 (2019) 103–112, https://doi.org/10.1016/j.spmi.2018.10.023.
[95] H.M.F. Ahmed, N.S. Begum, Synthesis and characterization of MoO_3-WO_3 composite thin films by liquid phase deposition technique: investigation of its photochromic properties, Bull. Mater. Sci. 36 (2013) 45–49, https://doi.org/10.1007/s12034-013-0422-y.
[96] S. Lek, P. Choopool, K. Kooptrnond, The photochromic properties of reduced graphene oxide doped tungsten/molybdenum trioxide nanocomposites, Dig. J. Nanomat. Biostr. 11 (2016) 821–831.
[97] Y. Tae, K.Y. Song, W.I. Lee, G.J. Choi, Y. Rag, Photocatalytic behavior of WO_3-loaded TiO_2 in an oxidation reaction, Semicond. Sci. Technol. 7 (1992) 423, https://doi.org/10.1006/jcat.1999.2776.
[98] T. He, M. Ying, H. Liu, G. Zhang, W. Yang, J. Yao, Photochromism of WO_3 Colloids combined with TiO_2 nanoparticles, J. Phys. Chem. 106 (2002) 12670–12676, https://doi.org/10.1021/jp026031t.
[99] S. Prabhu, L. Cindrella, O.J. Kwon, K. Mohanraju, Photoelectrochemical, photocatalytic and photochromic performance of rGO-TiO_2-WO_3 composites, Mater. Chem. Phys. 224 (2019) 217–228, https://doi.org/10.1016/j.matchemphys.2018.12.030.
[100] B.W. Faughnan, R.S. Crandall, P.M. Heyman, Electrochromism in tungsten(VI) oxide amorphous films, RCA Rev. 36 (1975) 177–197.
[101] A.I. Gavrilyuk, Photochromism in WO_3 thin films, Electrochim. Acta 44 (1999) 3027–3037.

[102] S. Lam, J. Sin, A. Abdullah, A. Mohamed, ZnO nanorods surface-decorated by WO_3 nanoparticles for photocatalytic degradation of endocrine disruptors under a compact fluorescent lamp, Ceram. Int. 39 (2013) 2343–2352, https://doi.org/10.1016/j.ceramint.2012.08.085.

[103] J. He, Q. Luo, Q.Z. Cai, X.W. Li, D.Q. Zhang, Microstructure and photocatalytic properties of WO_3/TiO_2 composite films by plasma electrolytic oxidation, Mater. Chem. Phys. 129 (2011) 242–248, https://doi.org/10.1016/j.matchemphys.2011.04.011.

[104] A.K.L. Sajjad, S. Sajjada, A. Iqbal, N.-A. Ryma, ZnO/WO_3 nanostructure as an efficient visible light catalyst, Ceram. Int. 44 (2018) 9364–9371, https://doi.org/10.1016/j.ceramint.2018.02.150.

[105] I. Andron, L. Marichez, V. Jubera, C. Labrugère, M. Duttine, C. Frayret, M. Gaudon, Photochromic behavior of ZnO/MoO_3 interfaces, ACS Appl. Mater. Interfaces 12 (41) (2020) 46972–46980, https://doi.org/10.1021/acsami.0c13335.

[106] S.K. Deb, J.A. Chopoorian, Optical properties and color-center Formation in thin films of molybdenum trioxide, J. Appl. Phys. 37 (1966) 4818–4825, https://doi.org/10.1063/1.1708145.

[107] I. Andron, L. Marichez, V. Jubera, A. Fargues, C. Frayret, M. Gaudon, Improvement of the photochromism taking place on ZnO/MoO_3 combined material interfaces, Mater. Adv. 2 (2021) 782–792, https://doi.org/10.1039/D0MA00896F.

[108] Ms J.A. Sobrinho, J.H.K.S. Monteiro, M.R. Davolos, M.A. Cebim, A.M. Pires, Photoluminescence and scintillation modulation upon UV/X-ray-Induced photochromism in europium tungstate phosphors, Chemistry Select 2 (2017) 3538–3548, https://doi.org/10.1002/slct.201700287.

[109] Q. Zhang, Y. Zhang, H. Sun, W. Geng, X. Wang, X. Hao, S. An, Tunable luminescence contrast of $Na_{0.5}Bi_{4.5}Ti_4O_{15}$:Re (Re = Sm, Pr, Er) photochromics by controlling the excitation energy of luminescent centers, ACS Appl. Mater. Interfaces 8 (2016) 34581–34589, https://doi.org/10.1021/acsami.6b11825.

[110] K. Li, L. Luo, Y. Zhang, W. Li, Y. Hou, The upconversion luminescence modulation and its enhancement in Er^{3+}-doped $Na_{0.5}Bi_{0.5}TiO_3$ based on photochromic reaction, J. Am. Ceram. Soc. 101 (2018) 5640–5650, https://doi.org/10.1111/jace.15879.

[111] Q.W. Zhang, J. Liu, H.Q. Sun, X.S. Wang, X.H. Hao, S.L. An, J. Mater. Chem. C 5 (2017) 807.

[112] Q.W. Zhang, H.Q. Sun, H. Li, X.S. Wang, X.H. Hao, S.L. Song, S.L. An, Chem. Commun. 97 (2015) 868.

[113] H. Sun, J. Liu, X. Wang, Q. Zhang, X. Hao, S. An, (K,Na)NbO_3 ferroelectrics: a new class of solid-state photochromic materials with reversible luminescence switching behavior, J. Mater. Chem. C 5 (2017) 9080–9087, https://doi.org/10.1039/C7TC03076B.

[114] Y. Zhang, J. Liu, H. Sun, D. Peng, R. Li, C. Bulin, X. Wang, Q. Zhang, X. Hao, Reversible luminescence modulation of Ho-doped $K_{0.5}Na_{0.5}NbO_3$ piezoelectrics with high luminescence contrast, J. Am. Ceram. Soc. 101 (2018) 2305–2312, https://doi.org/10.1111/jace.15389.

[115] Y. Zhang, L. Luo, K. Li, W. Li, Y. Hou, Light-controlled reversible photoluminescence modulation in photochromic Sr_2SnO_4 :Eu^{3+}, J. Phys. Appl. Phys. 51 (2018) 365102–365113, https://doi.org/10.1088/1361-6463/aad531.

[116] S. Kamimura, H. Yamada, C.-N. Xu, Purple photochromism in Sr_2SnO_4 :Eu^{3+} with layered perovskite-related structure, Appl. Phys. Lett. 102 (3) (2013), https://doi.org/10.1063/1.4788752, 031110-031115.

[117] Y. Zhang, L. Luo, K. Li, W. Li, Y. Hou, Reversible up-conversion luminescence modulation based on UV-VIS light-controlled photochromism in Er^{3+} doped Sr_2SnO_4, J. Mater. Chem. C 6 (48) (2018) 13148–13156, https://doi.org/10.1039/C8TC04725A.

[118] Y. Lv, S. Zhang, Z. Li, Y. Jin, H. Wu, G. Ju, L. Chen, Z. Hu, Y. Hu, Reversible multiplexing optical information storage and photoluminescence switching in Eu^{2+}-doped fluorophosphate-based tunable photochromic materials, J. Mater. Chem. C 9 (2021) 5930–5944, https://doi.org/10.1039/d1tc00759a.

[119] J. Guifang, Y. Hu, L. Chen, X. Wang, Photochromism of europium and gadolinium co-doped barium, ECS Solid. Stat. Lett. 1 (1) (2012) 1–3.

[120] Y. Lv, Z. Li, Y. Jin, H. Wu, C. Wang, G. Ju, L. Chen, Z. Hu, Y. Hu, A novel photochromic material based on halophosphate: remote lightcontrolled reversible luminescence modulation and fluorescence lifetime regulation, Ceram. Int. 45 (2019) 5971–5980, https://doi.org/10.1016/j.ceramint.2018.12.067.

[121] T. Yu Sizova, V. Yu Veslopolova, R. Yu Shendrik, A.V. Egranov, E.A. Radzhapov, A.A. Shalaev, Divalent rare-earth ions Pr, Sm, Ho, Er, Tm, and Yb in crystals of alkaline-earth fluorides, Bull. Russ. Acad. Sci. Phys. 81 (2017) 1090–1093, https://doi.org/10.3103/S1062873817090234.

[122] T. Sizova, E. Radzhabov, Photochromism in calcium and strontium fluoride crystals doped with rare-earths ions, IEEE Trans. Nucl. Sci. 59 (2012) 2098–2101, https://doi.org/10.1109/TNS.2012.2190423.

[123] R. Shendrik, A.S. Myasnikova, T.Y. Sizova, E.A. Radzhabov, Luminescence of photochromic centers in calcium fluoride crystals doped with Lu^{3+} ions, Radiat. Meas. 90 (2016) 127–131, https://doi.org/10.1016/j.radmeas.2015.12.042.

[124] Y. Jin, Y. Hu, Y. Fu, Z. Mu, G. Ju, Reversible white and light gray photochromism in europium doped Zn_2GeO_4, Mater. Lett. 134 (2014) 187–189, https://doi.org/10.1016/j.matlet.2014.07.084.

[125] Y. Lv, Y. Jin, C. Wang, L. Chen, G. Ju, Y. Hu, $Sr_3YLi(PO_4)_3$ F:Eu^{2+},Ln^{3+} : colorless-magenta photochromism and coloration degree regulation through Ln $^{3+}$ co-doping, RSC Adv. 7 (2017) 43700–43707, https://doi.org/10.1039/C7RA08090E.

[126] Y. Lv, Y. Jin, C. Wang, G. Ju, F. Xue, Y. Hu, Reversible white-purple photochromism in europium doped $Sr_3GdLi(PO_4)_3F$ powders, J. Lumin. 186 (2017) 238–242, https://doi.org/10.1016/j.jlumin.2017.02.052.

[127] Y. Jin, Y. Hu, Y. Fu, L. Chen, G. Ju, Z. Mu, Reversible colorless-cyan photochromism in Eu^{2+}-doped $Sr_3YNa(PO_4)_3F$ powders, J. Mater. Chem. C 3 (2015) 9435–9443, https://doi.org/10.1039/C5TC01797A.

[128] Y. Jin, Y. Lv, C. Wang, G. Ju, H. Wu, Y. Hu, Design and control of the coloration degree for photochromic $Sr_3GdNa(PO_4)_3F$:Eu^{2+} via traps modulation by Ln^{3+} (Ln = Y, La-Sm, Tb-Lu) co-doping, Sensor. Actuator. B Chem. 245 (2017) 256–262, https://doi.org/10.1016/j.snb.2017.01.129.

[129] R. Zhang, Y. Jin, L. Yuan, H. Wu, G. Xiong, C. Wang, L. Chen, Y. Hu, Photochromism of Sm^{3+}-doped perovskite oxide: ultrahigh-contrast optical switching and erasable optical recording, J. Lumin. 233 (2021) 117922, https://doi.org/10.1016/j.jlumin.2021.117922.

[130] C. Wang, Y. Jin, Y. Lv, G. Ju, L. Chen, Z. Li, Y. Hu, A bifunctional phosphor $Sr_3Sn_2O_7$:Eu^{3+}: red luminescence and photochromism properties, J. Lumin. 192 (2017) 337–342, https://doi.org/10.1016/j.jlumin.2017.07.004.

[131] L. Yuan, Y. Jin, D. Zhu, Z. Mou, G. Xie, Y. Hu, Ni^{2+}-Doped yttrium aluminum gallium garnet phosphors: bandgap engineering for broad-band wavelength-tunable shortwave- infrared long-persistent luminescence and photochromism, ACS Sustain. Chem. Eng. 8 (2020) 6543–6550, https://doi.org/10.1021/acssuschemeng.0c01377.

[132] Y. Jin, Y. Hu, L. Yuan, L. Chen, H. Wu, G. Ju, H. Duana, Z. Mu, Multifunctional near-infrared emitting Cr^{3+}-doped $Mg_4Ga_8Ge_2O_{20}$ particles with long persistent and photostimulated persistent luminescence, and photochromic properties, J. Mater. Chem. C 4 (2016) 6614–6625, https://doi.org/10.1039/c6tc01640e.

[133] Y. Yonezaki, S. Takei, Photochromism and emission-color change in $Ba_3MgSi_2O_8$-based phosphors, J. Lumin. 173 (2016) 237–242, https://doi.org/10.1016/j.jlumin.2016.01.026.

[134] Y. Yonezaki, S. Takei, K. Ogawa, Room-temperature emission-color switching of $Ba_3MgSi_2O_8$: Eu^{2+} and the photochemical reaction mechanism, J. Lumin. 188 (2017) 12–17, https://doi.org/10.1016/j.jlumin.2017.04.004.

[135] O.V. Kopyshinsky, B.A. Okhrimenko, S.E. Zelensky, B.A. Danilchenko, O. P. Shakhov, Laser-and γ-induced transformations of optical spectra of indium-doped sodium borate glass, J. Phys. Condens. Matter 15 (2003) 3919–3929, https://doi.org/10.1088/0953-8984/15/23/307.

[136] M.A. Buñuel, B. Moine, B. Jacquier, A. Garcia, J.P. Chaminade, Luminescence of In^+ in Ce^{3+} and Tb^{3+}-doped elpasolite-type fluoroindates, J. Appl. Phys. 86 (1999) 5045, https://doi.org/10.1063/1.371477.

[137] J.P. Chaminade, A. Garcia, T. Gaewdang, M. Pouchard, J. Grannec, B. Jacquier, Reversible photoionization process in luminescent Ce^{3+} doped elpasolite-type fluoroindates, Radiat. Eff. Defect Solid 135 (1995) 137–141, https://doi.org/10.1080/10420159508229823.

[138] L. Cornu, M. Gaudon, O. Toulemonde, P. Veber, V. Jubera, Optical contrast and cycling of bistable luminescence properties in $Rb_2KIn_{(1-x)}Ce_xF_6$ compounds, Dalton Trans. 45 (2016) 3380–3387, https://doi.org/10.1039/c5dt04772b.

[139] L. Cornu, M. Gaudon, P. Veber, A. Villesuzanne, S. Pechev, A. Garcia, V. Jubera, Discussion on the structure stability and the luminescence switch under irradiation of a Ce-doped elpasolite compound, Chem. Eur J. 21 (2015) 5242–5251, https://doi.org/10.1002/chem.201405784.

[140] Ines Andron, Thesis « Oxydes et fluorures photochromiques inorganiques : approches expérimentale et calculatoire », Université de Bordeaux, 2020. September 11th.